

Dual Location of the Mitochondrial Preprotein Transporters B14.7 and Tim23-2 in Complex I and the TIM17:23 Complex in *Arabidopsis* Links Mitochondrial Activity and Biogenesis

Yan Wang,^a Chris Carrie,^a Estelle Giraud,^a Dina Elhafez,^a Reena Narsai,^{a,b} Owen Duncan,^a James Whelan,^a and Monika W. Murcha^{a,1}

^aAustralian Research Council Centre of Excellence in Plant Energy Biology, University of Western Australia, Crawley 6009, Western Australia, Australia

^bCentre for Computational Systems Biology, University of Western Australia, Crawley 6009, Western Australia, Australia

Interactions between the respiratory chain and protein import complexes have been previously reported in *Saccharomyces cerevisiae*, but the biological significance of such interactions remains unknown. Characterization of two mitochondrial preprotein and amino acid transport proteins from *Arabidopsis thaliana*, NADH dehydrogenase B14.7 like (B14.7 [encoded by At2g42210]) and Translocase of the inner membrane subunit 23-2 (Tim23-2 [encoded by At1g72750]), revealed both proteins are present in respiratory chain complex I and the Translocase of the Inner Membrane 17:23. Whereas depletion of B14.7 by T-DNA insertion is lethal, Tim23-2 can be depleted without lethality. Subtle overexpression of Tim23-2 results in a severe delayed growth phenotype and revealed an unexpected, inverse correlation between the abundance of Tim23-2 and the abundance of respiratory complex I. This newly discovered relationship between protein import and respiratory function was confirmed through the investigation of independent complex I knockout mutants, which were found to have correspondingly increased levels of Tim23-2. This increase in Tim23-2 was also associated with delayed growth phenotypes, increased abundance of other import components, and an increased capacity for mitochondrial protein import. Analysis of the Tim23-2-overexpressing plants through global quantitation of transcript abundance and in-organelle protein synthesis assays revealed widespread alterations in transcript abundance of genes encoding mitochondrial proteins and altered rates of mitochondrial protein translation, indicating a pivotal relationship between the machinery of mitochondrial biogenesis and mitochondrial function.

INTRODUCTION

A variety of multisubunit protein complexes are present on the mitochondrial outer membrane (Translocase of the Outer Membrane [TOM] and Sorting and Assembly Machinery) (Stroud et al., 2010) and on the inner membrane (Translocase of the Inner Membrane 17:23 [TIM17:23] and TIM22) (Rehling et al., 2004; Mokranjac and Neupert, 2010), which act together to import the wide variety of mitochondrial proteins synthesized in the cytoplasm. Whereas the protein import apparatus is generally well conserved across phylogenetic groups (Hewitt et al., 2011), particularly the pore-forming subunits, which display high levels of orthology (Dolezal et al., 2006; Carrie et al., 2010a), significant differences have been observed between the outer mitochondrial membrane protein import receptors of plants compared with yeast

and mammals (Perry et al., 2006; Lister et al., 2007). Further differences include the location of the mitochondrial processing peptidase (MPP) in the cytochrome bc₁ complex (Braun et al., 1992; Glaser et al., 1994) in plants compared with yeast and mammals.

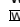
In the last decade, studies have revealed the higher order structure of multisubunit protein complexes on the mitochondrial inner membrane, in particular, the identification of respiratory chain supercomplexes (Stuart, 2008; Wittig and Schagger, 2009; Dudkina et al., 2010). Supercomplex structures between complex I and III, complex III and IV, dimeric ATP synthase, and even higher supercomplex structures have been described (Stuart, 2008; Dudkina et al., 2010; Sunderhaus et al., 2010). The functional significance of these respiratory supercomplexes is not yet clear; however, it has been proposed that these supercomplexes may enhance electron flow via substrate channeling, prevent the production of excess reactive oxygen species, or play a role in maintaining the stability of respiratory chain complexes (Dudkina et al., 2010; Sunderhaus et al., 2010). In the case of the ATP synthase complex, the arrangement of such supercomplexes is proposed to stabilize the cristae structure that is characteristic of the mitochondrial inner membrane (Wittig and Schagger, 2009; Dudkina et al., 2010).

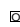
Similarly, protein import complexes have also been reported to form supercomplexes. Namely, the TIM17:23 complex has been reported to be associated with both the TOM complex and the presequence-assisted motor complex (PAM) (Schmidt et al.,

¹ Address correspondence to monika.murcha@uwa.edu.au.

The author responsible for distribution of materials integral to the findings presented in this article in accordance with the policy described in the Instructions for Authors (www.plantcell.org) is: Monika W. Murcha (monika.murcha@uwa.edu.au).

 Some figures in this article are displayed in color online but in black and white in the print edition.

 Online version contains Web-only data.

 Open Access articles can be viewed online without a subscription.

www.plantcell.org/cgi/doi/10.1105/tpc.112.098731

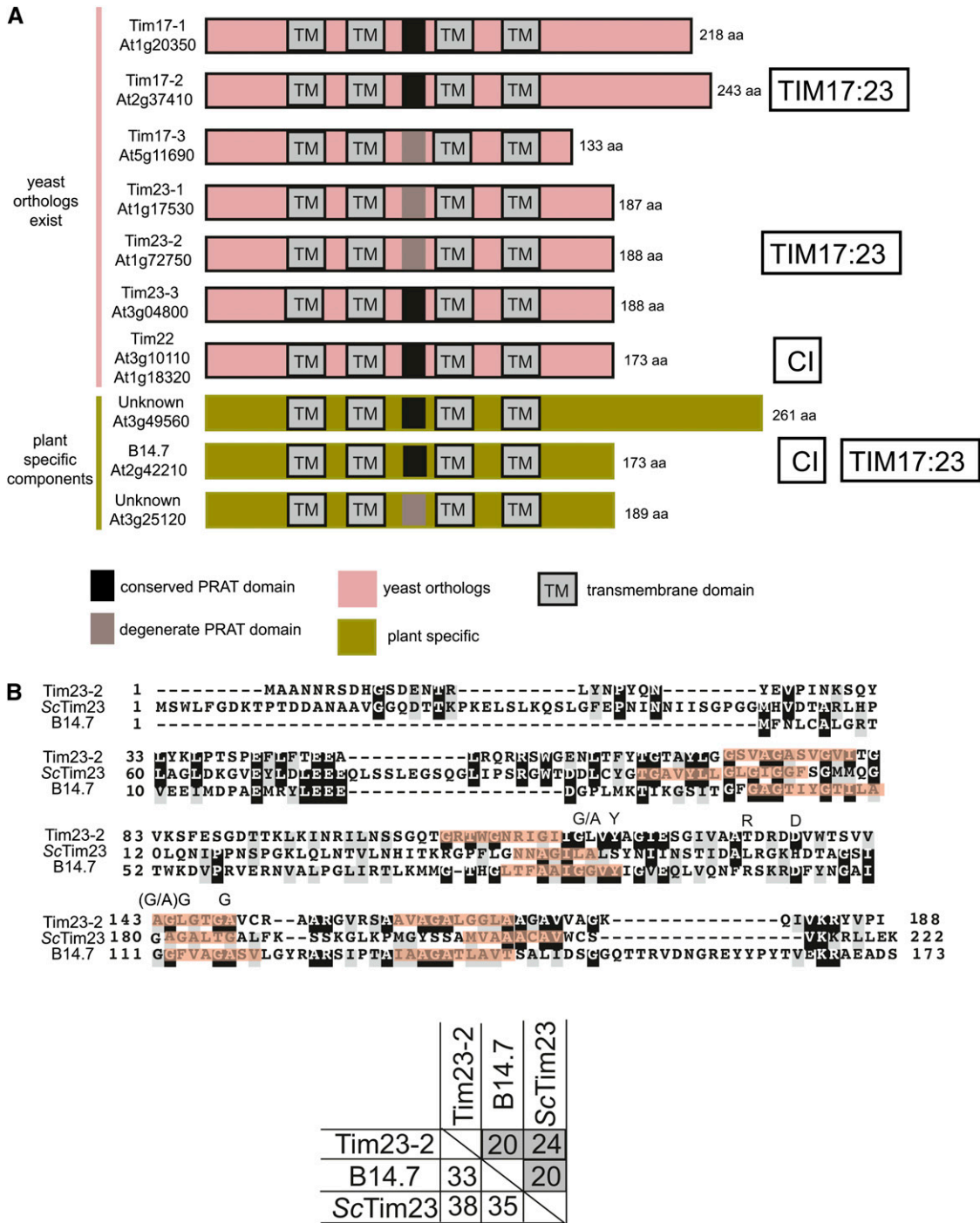


Figure 1. Overview of the PRAT Proteins in *Arabidopsis*.

(A) Diagrammatic representation of the 10 PRAT proteins previously shown to have a mitochondrial localization. The complex that these proteins have been identified in is indicated according to previous studies (Meyer et al., 2008; Klodmann et al., 2010, 2011). aa, amino acids.

(B) Comparison of sequences of Tim23-2 and B14.7 from *Arabidopsis* and Tim23 from *Saccharomyces cerevisiae* (Sc). The predicted transmembrane domains are highlighted, and the PRAT domain (G/A)₂(F/Y)₁X10RX3DX6(G/A/S)₁GX3G is indicated. Percentage identity (in gray) and similarity between Tim23-2, B14.7, and ScTim23.

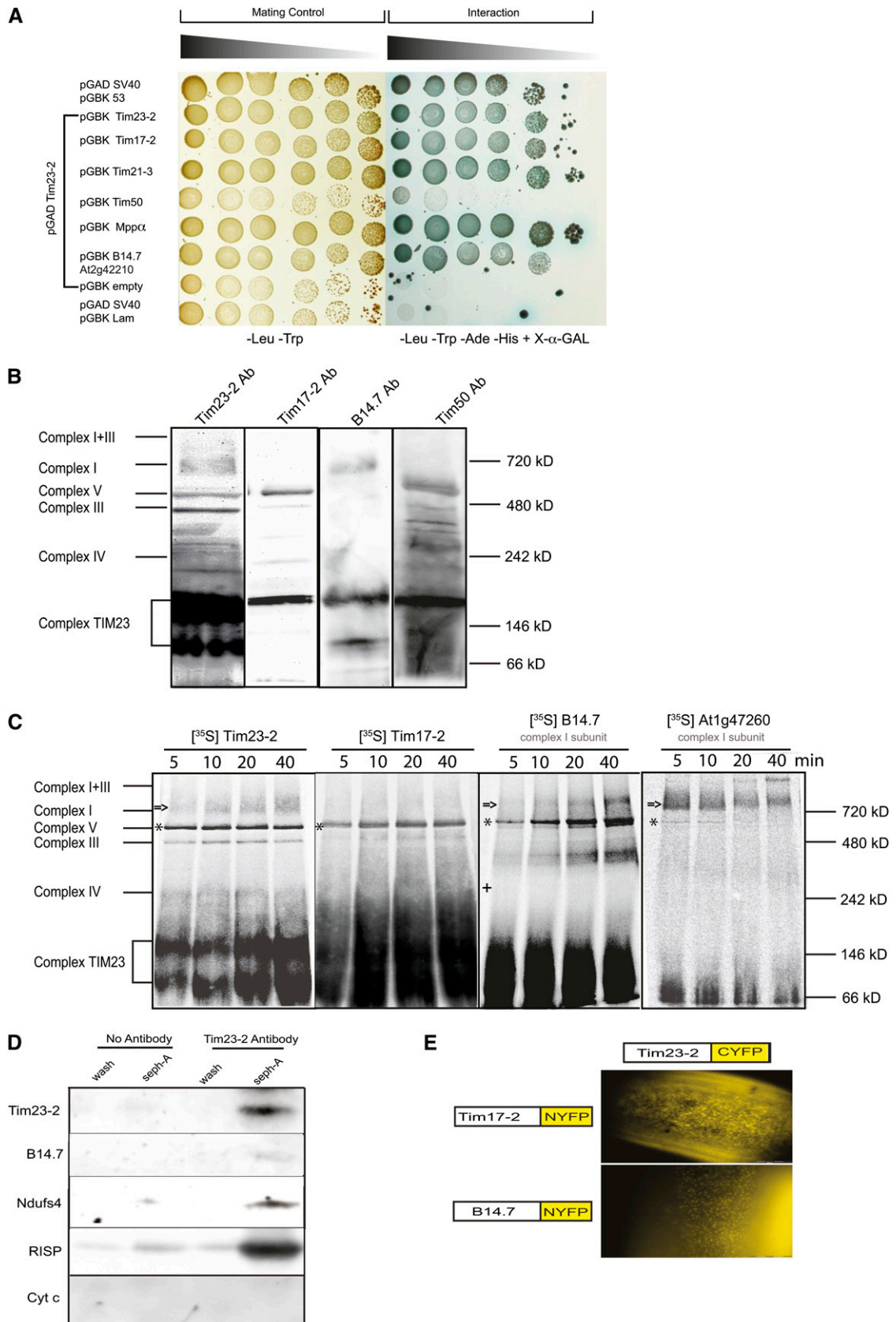


Figure 2. Interaction between TIM17:23 and Complex I.

2010). The PAM complex is located on the matrix side of the inner membrane and pulls precursor proteins through the TIM17:23 translocase into the matrix or inner membrane. Tim21, Tim23, and Tim50 play a role in facilitating interactions with the outer membrane TOM complex to form a dynamic TOM-TIM supercomplex (van der Laan et al., 2006; Chacinska et al., 2010). In fact, two distinct forms of TIM17:23 have been identified, TIM17:23^{sort} and TIM17:23^{motor} (Schmidt et al., 2010). TIM17:23^{sort} contains Tim17, 23, 50, and 21 and is involved in the lateral insertion of preproteins into the inner membrane (Schmidt et al., 2010). TIM17:23^{motor} translocates proteins into the matrix and does not contain Tim21 but does contain the PAM subunits Tim44, HSP70, Mge1, and Pam 16, 17, and 18 (Schmidt et al., 2010).

There are also a number of reports of respiratory chain components and protein import complexes interacting or converging via two types of interactions. First, protein subunits in a respiratory chain complex have been reported to be involved in protein import, this was initially reported with the finding that a subunit of the matrix-located MPP (β -MPP) also functions as one of the core subunits of the cytochrome bc_1 complex in *Neurospora crassa* (Schulte et al., 1989). Further studies in plants revealed a unique evolutionary history for MPP in mitochondria (Braun et al., 1992; Glaser et al., 1994; Eriksson et al., 1996; Brumme et al., 1998; Glaser and Dessi, 1999), where the core subunits of plant cytochrome bc_1 complexes are bifunctional, acting as both a peptidase and as integral subunits of the cytochrome bc_1 complex (Braun et al., 1992; Eriksson et al., 1996). More recently, it has been reported that the succinate dehydrogenase subunit 3 in yeast is also a component of the TIM22 translocase and has an active role in the import of proteins via the carrier import pathway (Gebert et al., 2011). The second type of interaction is where the multisubunit protein complexes interact to form supercomplexes; for example, current evidence indicates that Tim21 mediates the interaction between the TIM17:23 and complex III in yeast (van der Laan et al., 2006).

Arabidopsis thaliana contains 17 genes encoding proteins that belong to the Preprotein and Amino acid Transport family (PRAT) (Rassow et al., 1999), of which 10 proteins are located in mitochondria, six are located in plastids, and one protein is dual targeted to mitochondria and plastids (Murcha et al., 2007). Of

the 10 mitochondrial PRAT proteins, phylogenetic analysis suggested that three genes encode Tim17, three genes encode Tim23, two identical genes encode Tim22, and three genes encode proteins of unknown function (Murcha et al., 2007). One of these genes (At2g42210) encoding a protein of unknown function was subsequently shown to encode the complex I subunit B14.7 (Meyer et al., 2008; Klodmann et al., 2010; Klodmann et al., 2011). Complex I from *N. crassa*, humans, and *Chlamydomonas reinhardtii* have also been shown to contain a subunit that is similar to the PRAT family proteins, namely, *N. crassa* 21.3b (GenBank/P25710), human NDUFA11, and *C. reinhardtii* v2.0/C_180167 (GenBank/AAS58499) (Nehls et al., 1991; Carroll et al., 2002; Murray et al., 2003). In *Arabidopsis*, this protein has been identified to be a single peripheral subunit of complex I in two independent studies, both of which identified B14.7 in stoichiometric amounts by proteomic analysis (Meyer et al., 2008; Klodmann et al., 2010).

To investigate the extent and implications of any interactions between the respiratory chain and protein import complexes on the inner mitochondrial membrane, the locations and the interactions of various components of the TIM17:23 complex in *Arabidopsis* were investigated. The biological implications of interactions between respiratory chain complexes and the mitochondrial protein import machinery are unclear in plants. While yeast is an excellent simple eukaryotic model system, it differs from plants in many aspects with reference to mitochondrial biology, most notably that it lacks a complex I. In this study, we describe an interaction between TIM17:23 and respiratory complex I. Furthermore, the stoichiometric amounts of these two complexes are linked in vivo and may provide a link between protein import and respiration to regulate mitochondrial biogenesis in plants.

RESULTS

Interaction between Tim23 and Complex I

Of the 10 mitochondrial PRAT proteins (Murcha et al., 2007), two have been reported to be located in complex I of the respiratory chain (Figure 1A). Tim22 was shown to migrate with complex I,

Figure 2. (continued).

(A) Yeast two-hybrid interaction assays indicate a positive interaction of Tim23-2 with complex I subunit B14.7. The yeast strain AH109, transformed with pGADT7 Tim23-2, was mated with yeast strain Y187, transformed with either pGBKT7 Tim17-2, Tim23-2, Tim50, Tim21, complex III subunit MPP α , complex I subunit B14.7, or empty vector pGBKT7. Diploid yeast growth on $-Trp -Leu$ media indicates successful mating. Growth on $-Trp -Leu -Ade -His$ with X- α -D-galactoside indicates specific protein-protein interactions.

(B) Immunodetection of Tim23-2, Tim17-2, B14.7, and Tim50 in total mitochondrial proteins separated by BN-PAGE. Nonspecific bands are indicated by an asterisk.

(C) BN-PAGE of time-course analysis of the import into mitochondria of radiolabeled Tim23-2, Tim17-2, complex I subunit B14.7, and complex I subunit encoded by At1g47260. Incorporation of radiolabeled protein into complex I is indicated by arrows, nonspecific incorporation into complex V is indicated by asterisks, and nonspecific incorporation of B14.7 into an unknown complex is indicated by a plus sign.

(D) Mitochondrial proteins isolated from Col-0 (wild-type) plants were incubated with or without antibodies raised against Tim23-2 and Protein A-Sepharose. The wash and pellet fractions were resolved by SDS-PAGE and immunodetected with antibodies against Tim23-2, B14.7, complex I subunit Ndufs4, complex III subunit RISP, and cytochrome c.

(E) Interaction of Tim23-2 with Tim17-2 and B14.7 was determined by BiFC in onion epidermal cells using biolistic transformation. YFP, yellow fluorescent protein.

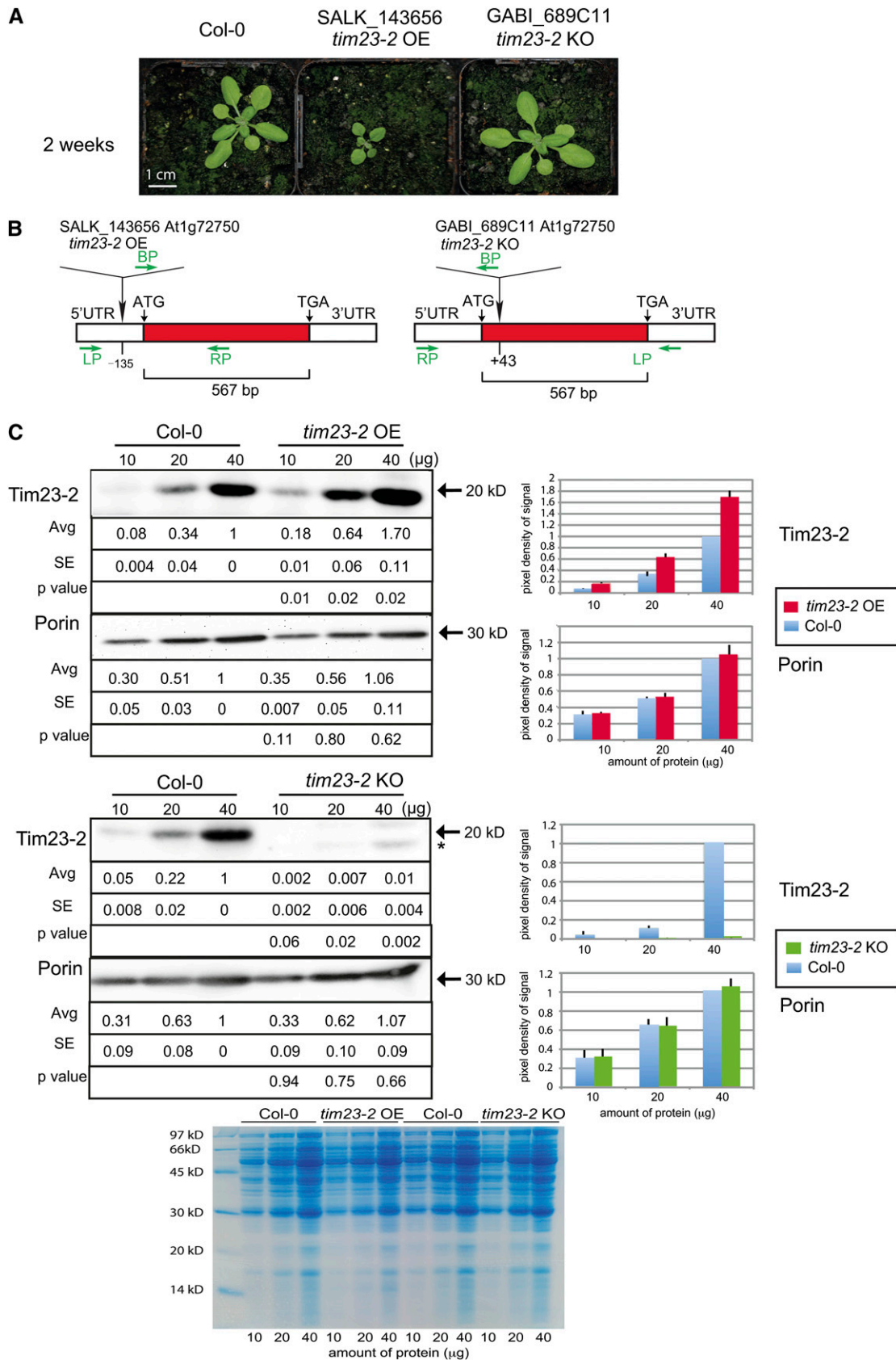


Figure 3. Overexpression of Tim23-2 Results in a Retarded Growth Phenotype.

(A) Growth phenotypes for *Arabidopsis* plants that contain T-DNA insertions annotated to be located in *Tim23-2* (At1g72750) at 2 weeks old.

while the complex I subunit B14.7 (Meyer et al., 2008; Klodmann et al., 2010), migrates with both complex I and the TIM17:23 complex (Klodmann et al., 2011; Rode et al., 2011). A comparison of B14.7, Tim23-2, and yeast Tim23 shows that B14.7 is similar to yeast Tim23 in terms of overall characteristics and contains an Arg residue in the correct position of the PRAT consensus domain, G/AX₂F/YX₁₀RX₃DX₆G/A/SGX₃G, compared with Tim23-2 (Figure 1B). It has been shown that this Arg residue must be inserted into Tim23-2 from *Arabidopsis* before it can complement a *tim23* yeast deletion strain (Murcha et al., 2003). To confirm that B14.7 was present in both complex I and TIM17:23, a variety of assays were used both to test for interactions of B14.7 with TIM17:23 and to determine whether B14.7 was a subunit of TIM17:23.

Proteins of the TIM17:23 complex from *Arabidopsis* were used to probe for protein–protein interactions using yeast two-hybrid assays. Tim23-2 was tested for interactions against various components of the TIM17:23 complex and complex I and complex III subunits (Figure 2A). Proteins known to interact with Tim23-2, such as Tim23-2 itself, Tim17-2, and Tim50, displayed positive interactions, evidenced by growth on –Leu –Trp –Ade –His with X- α -D-galactoside and a blue phenotype (Figure 2A). Tim23-2 was found to interact with the complex III subunit, MPP α , and the complex I subunit, B14.7 (Figure 2A) (Meyer et al., 2008; Klodmann et al., 2010). The empty vector alone exhibited growth only on –Leu –Trp media, confirming that the growth observed on selection media was due to specific interactions of Tim23-2 (and Tim17-2) with partner proteins.

Whereas the yeast two-hybrid assays showed that B14.7 can interact with Tim23-2 (Figure 2A), this does not directly indicate that B14.7 is a subunit of TIM17:23 or confirm the previous report that B14.7 comigrates with TIM17:23 (Klodmann et al., 2011; Rode et al., 2011). This was determined in two ways: by probing protein complexes separated by Blue-Native PAGE (BN-PAGE) with a variety of antibodies (Figure 2B) and by analyzing the ability of radiolabeled proteins to be incorporated into protein complexes (Figure 2C). Antibodies raised against Tim23-2 detected two protein bands with apparent molecular masses of ~100 and ~200 kD (Figure 2B). In addition to several non-specific interactions (indicated by an asterisk), a band was consistently detected at ~720 kD, which represents the mobility of monomeric complex I. Probing with Tim17-2 antibody detected the single TIM17:23 complex at ~200 kD, and no cross-reaction was observed at ~720 kD, which corresponds with the location of complex I (Figure 2B). The antibody raised against B14.7 similarly cross-reacted with the Tim17:23 complex at ~100 and ~200 kD in addition to the monomeric complex I (Figure 2B). The specificity of the antibody to B14.7 was determined against recombinant full-length Tim23-1, Tim23-2, and

Tim23-3 proteins, and no cross-reactivity was observed (see Supplemental Figure 1 online). An antibody raised against Tim50 also detected the upper band of Tim17:23 complex, but not complex I (Figure 2B). To confirm further the dual locations of both Tim23-2 and B14.7, in vitro protein uptake assays of radiolabeled proteins were performed and analyzed by BN-PAGE. The uptake of radiolabeled Tim23-2 into the Tim17:23 complexes was observed as expected, but uptake of Tim23-2 into the monomeric complex I was also distinctly observed, in a manner that increased over time (Figure 2C). In the case of Tim17-2, whereas import into the TIM17:23 complexes was similarly observed, there was no incorporation of radiolabeled protein into complex I (Figure 2C). For B14.7, uptake was observed into the TIM17:23 complex and complex I in a time-dependant manner, whereas another complex I subunit, encoded by At1g47260, was shown to incorporate into both monomeric complex I and the supercomplex I+III (Figure 2C). Incorporation of B14.7 was also observed into an unknown complex, located between complex III and complex IV (Figure 2C, indicated with a +). In addition, nonspecific labeling of complex V was observed with all precursor proteins (indicated by an asterisk), which likely represents the incorporation of radiolabeled Met into subunit 9 and the α -subunit of the ATP synthase complex that are encoded in the mitochondrion. While unlabeled Met is added prior to the import assay, it is not unexpected that some incorporation can still occur (Carrie et al., 2010b). These results suggest that both Tim23-2 and B14.7 are imported into and accumulate in both complex I and the TIM17:23 complex.

The interaction of Tim23-2 with complex I was further confirmed by immunoprecipitation and bimolecular fluorescence complementation (BiFC) (Figures 2D and 2E). Mitochondria isolated from Columbia-0 (Col-0) plants were lysed and immunoprecipitation was performed with antibodies raised against Tim23-2. In addition to Tim23-2 and B14.7 being detected in the precipitated products (Figure 2D), the complex I subunit Ndufs4 and complex III subunit Rieske Iron-Sulfur protein (RISP) were also detected, while cytochrome c was not, indicating that antibodies to Tim23-2 can specifically pull down complex I and complex III subunits. Using a split yellow fluorescent protein BiFC assay, the interaction of Tim23-2 with the B14.7 was confirmed and found to be mitochondrial in location by biolistic transformation in onion (*Allium cepa*) epidermal cells (Figure 2E).

Finally, it has been reported previously that in yeast, Tim21 interacts with complex III (van der Laan et al., 2006). Using a similar set of assays, interaction between Tim21 (encoded by At4g00026) and the cytochrome bc₁ complex was revealed in *Arabidopsis* (see Supplemental Figure 2 online). However, as yeast mitochondria lack complex I, and instead use a type II NADH dehydrogenase (Melo et al., 2004), this interaction between

Figure 3. (continued).

(B) The positions of the T-DNA inserts in SALK_143656 and GABI_689C11 lines. UTR, untranslated region.

(C) Mitochondria isolated from wild-type (Col-0), SALK_143656 (*tim23-2* OE), and GABI_689C11 (*tim23-2* KO) were subjected to SDS-PAGE and probed with antibodies raised against Tim23-2 and Porin (see Supplemental Figure 3A online). The apparent molecular mass of the protein detected is indicated. The 20-kD band is consistent with previous analysis of in vitro synthesized and imported Tim23-2 (Murcha et al., 2005b). Coomassie blue staining shows equal loading of protein.

complex I and TIM17:23 has not been previously shown in other systems. Therefore, we further investigated this interaction using genetic approaches to determine the biological significance.

Genetic Characterization of the Interactions between Tim17-2, Tim23-2, and B14.7

To characterize the interactions between Tim17-2, Tim23-2, and B14.7, T-DNA insertion lines were screened for each protein. In the case of Tim17-2 and B14.7, no homozygous lines could be obtained, indicating these are essential proteins in *Arabidopsis*. As *tim17* is an essential gene in yeast, it is not unexpected that such lethality was also observed in *Arabidopsis* (Dekker et al., 1993; Maarse et al., 1994). Interestingly, previous studies have characterized complex I-deficient mutants from tobacco (*Nicotiana tabacum*) and *Arabidopsis* and revealed that these plants are viable but exhibit a retarded growth phenotype (Dutilleul et al., 2003; Meyer et al., 2009). Therefore, the lethality of the knockout for B14.7 suggests that it may have other essential roles, in addition to being a complex I subunit.

Two viable T-DNA insertion lines (SALK_143656 and GABI_689C11) were obtained for Tim23-2 (Figure 3A). However, while one line displayed an apparently normal growth phenotype (GABI_689C11), the other line (SALK_143656) displayed a severe delayed growth phenotype throughout the life cycle (Figure 3A). This apparent discrepancy was resolved by mapping and sequencing of the T-DNA insertion in both lines, which revealed that whereas one line (GABI_689C11) represented an insertion in the gene at position 43 bp 3' (downstream) of the translational start site, the insertion for the other line (SALK_143656) was in fact located 135 bp 5' (upstream) of the translational start site (Figure 3B). To determine the effect of both insertions on the

abundance of Tim23-2 protein, antibodies raised against Tim23-2 were used in quantitative immunoblot analysis of mitochondria isolated from each line (Figure 3C). In SALK_143656, in which the T-DNA was inserted 135 bp upstream of the translation start site and which exhibited a retarded growth phenotype (Figures 3A and 3B), there was a significant increase (ranging from 1.7- to 2.25-fold; $P < 0.05$) in abundance of Tim23-2 protein (Figure 3C). By contrast, the same Tim23-2 protein quantitation in the T-DNA insertion line GABI_689C11, where the T-DNA insert is located at a position 43 bp 5' of the gene, resulted in no Tim23-2 protein detected with an apparent molecular mass of 20 kD; instead, a smaller unique band of 18 kD was detected (indicated by an asterisk, Figure 3C). Thus, these lines are referred to as knockout (*tim23-2* KO) for GABI_689C11 and overexpressor (*tim23-2* OE) for SALK_143656.

The specificity of the Tim23-2 antibody, which was raised against amino acid regions 3 to 32 and 103 to 143, was verified using recombinant full-length overexpressed protein for all three Tim23 isoforms (see Supplemental Figure 3A online). The Tim23-2 antibody cross-reacted against both recombinant Tim23-1 and Tim23-2. Thus, it was not possible to distinguish between Tim23-1 and Tim23-2 using the Tim23-2 antibody alone. An additional antibody raised against Tim23-3 (amino acids 6 to 32 and 64 to 132) detected both recombinant Tim23-1 and Tim23-3 proteins but not Tim23-2 (see Supplemental Figure 3A online). Using the Tim23-3 antibody, no signal was detected in immunoblot analysis of mitochondria isolated from Col-0 plants or any of the Tim23 T-DNA lines (see Supplemental Figure 3A online), implying that Tim23-1 and Tim23-3 are not present in detectable amounts in mitochondria under the conditions tested in this study.

Notably, probing mitochondria isolated from the *tim23-2* KO line with the Tim23-2 antibody detected a weak band, corresponding

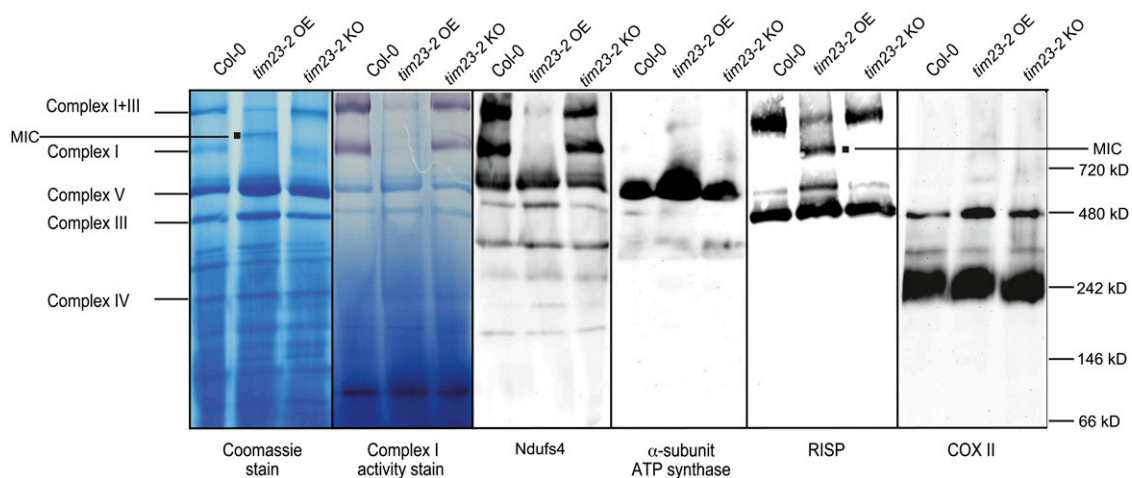


Figure 4. Complex I Is Reduced in *tim23-2* OE Mutant.

Mitochondria were isolated from Col-0 (wild-type), *tim23-2* OE, and *tim23-2* KO lines and resolved by one-dimensional BN-PAGE, stained with Coomassie blue, and analyzed for complex I activity. The bands corresponding to the supercomplex I+III, complex I, complex V, complex III, and complex IV are indicated. Immunodetection of complex I subunit Ndufs4, complex V α -subunit of ATP synthase, complex III subunit RISP, and complex IV subunit cytochrome oxidase II (COXII). The presence of an additional complex in the *tim23-2* OE line termed MIC was also detected by Coomassie blue staining and the RISP antibody as indicated with a black box.

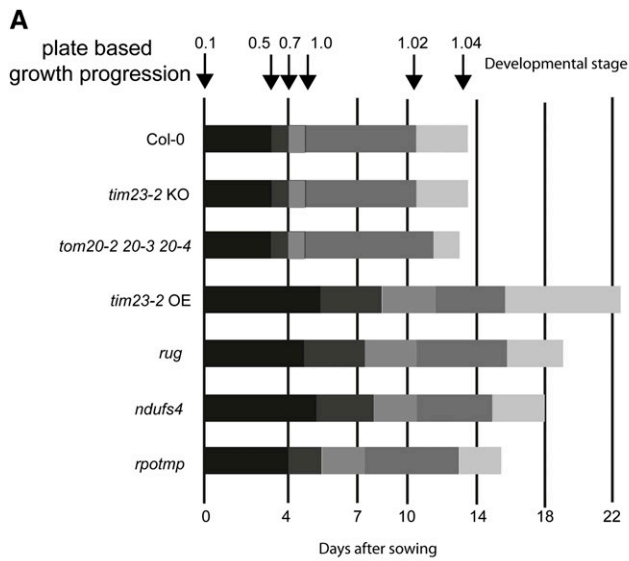
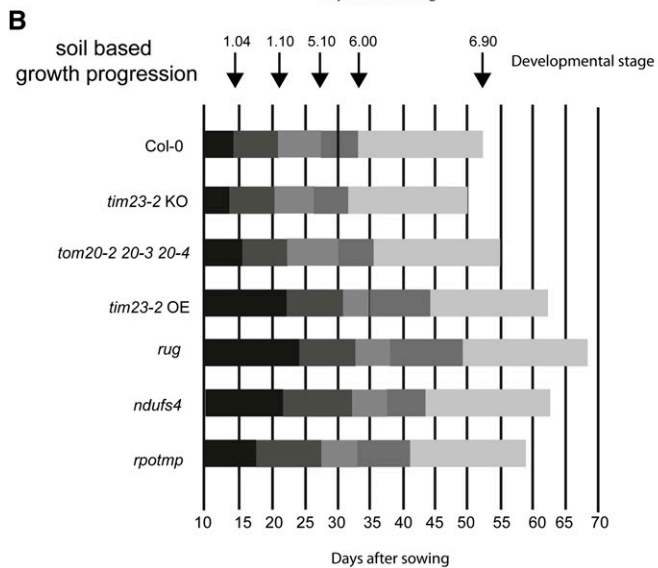
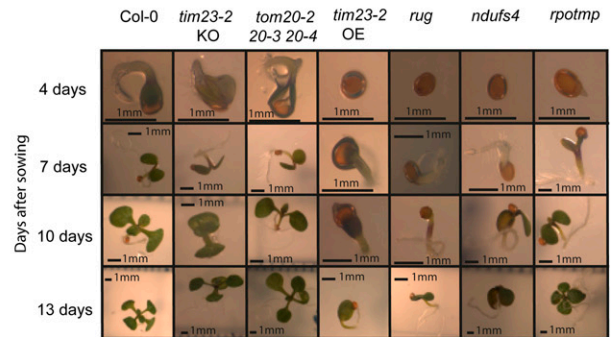


plate based growth progression



soil based growth progression

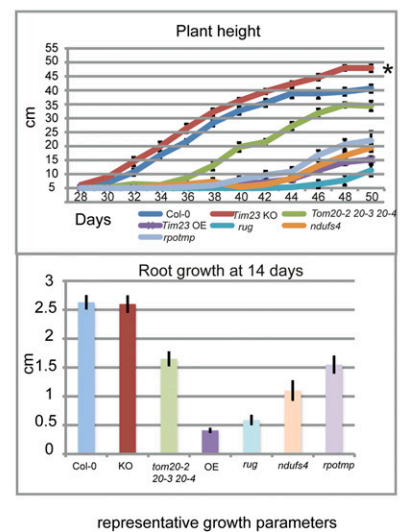
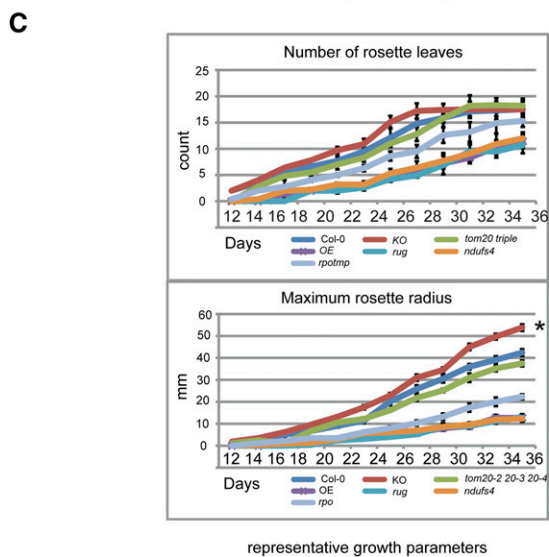
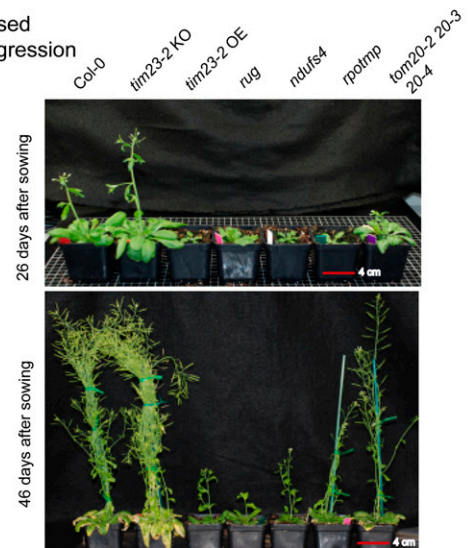


Figure 5. Growth Stage Analysis of *tim23-2* OE, *tim23-2* KO, Complex I Mutant Lines, *rug*, *ndufs4*, and *rpotmp* and *tom20* Triple Mutant.

to a smaller protein of ~18 kD in size, which is not evident in Col-0 or *tim23-2* OE blots (Figure 3C). Analysis of the transcript abundance for *Tim23-2* revealed that for the *tim23-2* KO line, the T-DNA insertion at position 43 bp results in elevated amounts of *Tim23-2* transcript downstream of the T-DNA insert. This is in agreement with the detection of a smaller protein likely to represent a truncated form of *Tim23-2*, translated downstream of the T-DNA insert (see Supplemental Figure 3B online). In the case of the *tim23-2* OE line, while *Tim23-2* transcript abundance was not elevated, and even somewhat reduced (see Supplemental Figure 3B online), protein abundance was increased (Figure 3C). Previous studies in rice (*Oryza sativa*) and *Arabidopsis* have reported that changes in the protein abundances of components of the mitochondrial protein import apparatus are generally not accompanied by changes in the respective transcript abundances. This was observed during germination in rice (Howell et al., 2006) and between aerobically and anaerobically grown rice (Howell et al., 2007). Similarly, in *Arabidopsis*, the mitochondrial protein import components do not show a correlation between changes in protein and transcript abundance during germination (Law et al., 2012). In addition, the inactivation of any *Tom20* or *OM64* genes, which encode the receptor components of the TOM complex, has been shown to result in an increase in protein abundance of other isoforms, without any change seen in transcript abundance (Lister et al., 2007). Thus, the amount of *Tim23-2* in the *tim23-2* OE line appears to be regulated posttranscriptionally.

To investigate further possible reasons for the observed growth defect of *tim23-2* OE plants, mitochondria from Col-0, *tim23-2* OE, and *tim23-2* KO lines were analyzed by BN-PAGE. Analysis of the Coomassie blue-stained gel showed that there was a difference in the banding pattern observed for Col-0, *tim23-2* OE, and *tim23-2* KO mitochondria (Figure 4). Mitochondria from Col-0 plants showed the characteristic pattern of the respiratory chain complexes, with both the monomeric complexes I and III and the supercomplex I+III evidenced (Figure 4). The monomeric form of complex I appears to be absent in the *tim23-2* OE line, while the supercomplex I+III is greatly reduced in abundance (Figure 4). An additional band, between the supercomplex I+III and complex I was observed (Figure 4, black square) and termed mixed intermediate complex (MIC), which comprises a mixture of inner membrane complex components, such as subunits of complex I, III, V, and prohibitin (see Supplemental Figure 4 online). The pattern of protein complexes from *tim23-2* KO plants were similar to Col-0 plants, except that

the monomeric form of complex I appeared slightly diffused (Figure 4). An activity stain for complex I, analyzed by BN-PAGE, confirmed the reduction of complex I in *tim23-2* OE, although it is notable that some activity is still present, especially at the supercomplex I+III (Figure 4). Immunoblot analysis, using an antibody specific for the complex I subunit, *Ndufs4*, confirmed that complex I was severely reduced in the *tim23-2* OE line (Figure 4). The mobility and amount of complex IV was unchanged when detected with antibodies against the complex IV subunit, COXII. Probing with antibodies against the complex III subunit, RISP, showed a reduction in the supercomplex of complex I+III and the presence of this subunit in the MIC complex (Figure 4). Also, while the intensity of complex III appears to have increased, as determined by the intensity of the band probed with the RISP antibody, this may be explained in part by the absence of the supercomplex I+III. An increase in the abundance of the complex V α -subunit of ATP synthase was also observed in the *tim23-2* OE line (Figure 4).

The data above suggests that the growth defect observed within the *tim23-2* OE plants occurred as a result of a reduction in the amount of complex I. Thus, we characterized several other mutant lines where complex I activity had been dramatically reduced. Three independent complex I mutants, *rug*, *ndufs4*, and *rpotmp*, were used and growth analysis was performed and compared with *tim23-2* OE plants. Additionally, as *tim23-2* KO appeared to have no deleterious growth defect, it was also included in the growth analysis. Finally, a triple mutant for the *tom20* outer membrane preprotein receptor that displays significantly reduced rates of protein import (Lister et al., 2007) was also used for comparison. The *tim23-2* OE line displayed a similar delayed growth phenotype to the complex I mutants when grown on plates and soil (Figures 5A and 5B), and as expected, the *tim23-2* KO plants displayed growth characteristics more similar to Col-0 (Figures 5A and 5B), reaching defined development stages earlier than Col-0 (Figure 5B), with plant height, and maximum rosette radius even observed to be significantly greater than Col-0 ($P < 0.05$) (Figure 5C). Based on these findings, phenotypically the *tim23-2* OE is most similar to complex I mutants.

Overexpression of *Tim23-2* and Complex I Mutants Shows Increased Rates of Protein Import

As *Tim23* is the channel forming subunit in the TIM17:23 translocase in yeast (Truscott et al., 2001), we investigated whether

Figure 5. (continued).

- (A)** Plate-based growth progression analysis of Col-0, *tim23-2* KO, *tom20-2 20-3 20-4* (*tom20* triple mutant), *tim23-2* OE, *rug ndufs4*, and *rpotmp*. Arrows define the time (days after sowing) that Col-0 plants have reached the growth stages as defined by Boyes et al. (2001). Boxes define the time between the growth stages, and shading indicates the occurrence of each growth stage. Stage 0.1, imbibition; stage 0.5, radical emergence; stage 0.7, hypocotyl emerge from seed coat; stage 1.0, cotyledons fully opened; stage 1.02, two rosette leaves >1 mm in length; stage 1.04, four rosette leaves >1 mm in length. Data are given as averages for 10 plants. Days are relative to the days after sowing after a 3-d stratification at 4°C
- (B)** Soil-based growth progression as in **(A)**: stage 1.10, 10 rosette leaves >1 mm; stage 5.10, first flower buds visible; stage 6.00, first flower opens; stage 6.90, flowering complete.
- (C)** Representative growth parameters of Col-0 and mutants, number of rosette leaves >1 mm, maximum rosette radius (mm) over time, plant height (cm) over time, and root length (cm) at 14 d. Data are given as averages \pm SE for 10 plants. $P < 0.05$ using a Student's *t* test.

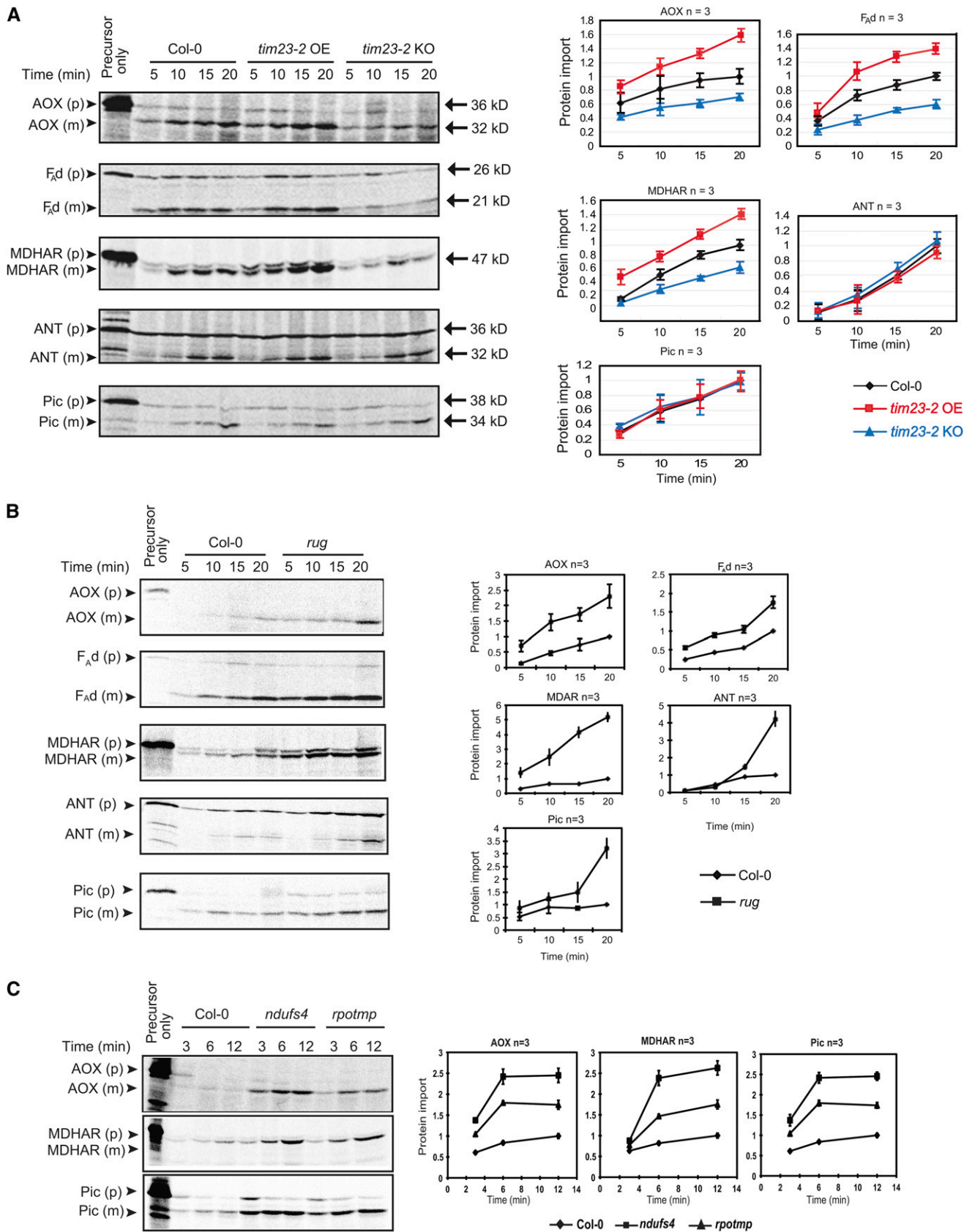


Figure 6. Overexpression of Tim23-2 or a Decrease in Complex I Results in Increased Import Ability.

protein import was affected in the *tim23-2* KO and OE lines in *Arabidopsis*. Three proteins that contain N-terminal cleavable targeting signals and are imported via the general import pathway were used including the alternative oxidase (AOX) (Whelan et al., 1995), the F_{AD} subunit of ATP synthase (F_{AD}) (Smith et al., 1994), and the dual-targeted protein monodehydroascorbate reductase (MDHAR) (Chew et al., 2003). Protein import via the carrier import pathway was also tested using the adenine nucleotide carrier (ANT) and the phosphate carrier (Pic) (Murcha et al., 2005b). The *tim23-2* OE line exhibited an increase in the import ability of AOX, F_{AD} , and MDHAR, while mitochondria isolated from *tim23-2* KO plants displayed a reduced import ability of these three precursor proteins (Figure 6A). The effect of altered Tim23-2 levels was seen to be specific to precursor proteins imported via the general import pathway, as no differences were observed with the import of ANT or Pic (Figure 6A), which are both precursors of the carrier import pathway (Murcha et al., 2005b). Thus, while overexpression of Tim23-2 protein resulted in an increased import ability via the general import pathway, it is not clear why a retarded growth phenotype was observed.

Characterization of the import capacity of mitochondria isolated from the complex I mutants also displayed an increase in protein import (Figures 6B and 6C). The *rug* mutant line revealed increased import ability of all proteins tested via both the general import pathway (AOX, F_{AD} , and MDHAR) and the carrier import pathway (ANT and Pic) (Figure 6B). The latter differs from the *tim23-2* OE line, in that there was no increase in the import ability of carrier pathway proteins (Figure 6A, ANT and Pic panels versus Figure 6B, ANT and Pic panels). Similarly, the import ability of the *ndufs4* mutant line and to a lesser extent the *rpotmp* line, exhibited increased import ability of AOX, MDHAR, and Pic precursor proteins when compared with Col-0 (Figure 6C).

A Reduction in Complex I Results in an Increase in Tim23

To further investigate the similarities between the *tim23-2* OE plants and the complex I mutant plants, mitochondria were isolated from Col-0, *tim23-2* KO, *tim23-2* OE, *rug*, *ndufs4*, and *rpotmp* plants and probed with a series of antibodies raised against mitochondrial PRAT proteins (Murcha et al., 2007), respiratory chain components, and proteins involved in protein import (Figure 7). Antibody dilutions were optimized for specific concentrations to ensure linearity of detection against Col-0 mitochondria (see Supplemental Figure 5 online). Interestingly,

probing mitochondria isolated from these lines, with antibodies to Tim23-2, revealed that all complex I mutants displayed an increase in Tim23-2 protein abundance, similar to that of mitochondria isolated from the *tim23-2* OE plants (Figure 7A).

In the case of other mitochondrial PRAT proteins, it was evident that an increase or decrease in the amount of Tim23-2 was accompanied by similar variations in Tim17-2 protein abundance (Figure 7A). For B14.7, a subunit of complex I and a PRAT protein, abundance decreased only slightly in the *tim23-2* KO line and increased in the *tim23-2* OE and *ndufs4* lines. B14.7 protein was not detected in the *rug* mutant plants and was only barely detected in the *rpotmp* mutant plants (Figure 7A). This indicates that while a T-DNA insertion into the locus At2g42210 (encoding B14.7) is lethal, even the reduced amounts of the protein that were detected in the *rug* line and *rpotmp* lines are sufficient to restore viability. As complex I is still largely absent in these lines, it further supports a dual role for B14.7, one in complex I and a second role in the TIM17:23 complex, that is essential for viability. A PRAT protein of unknown function encoded by At3g25120 showed slight increases in abundances in all lines, including in the *tim23-2* KO line (Figure 7A). Tim22, a protein encoded by At3g10110 or At1g18320 (two genes which have 100% identity), which has been shown to complement a yeast *tim22* deletion mutant (Murcha et al., 2007), also increased in abundance in the *tim23-2* OE and complex I mutant lines (Figure 7A).

Analysis of a variety of protein import components revealed an increase in Tim44 protein abundance in all lines (Figure 7B). In addition, all three Tom20 isoforms increased in abundance in all lines. Increases were also observed in the abundance of Sam50, Tim50, Tim21, and Tim9, most prominently in the *tim23-2* KO, OE, and *rug* lines (Figure 7B).

In the case of a variety of other respiratory chain components, the most notable effect observed was a >80% reduction in Ndufs4 protein abundance in the *tim23-2* OE, *rug*, and *rpotmp* lines (Figure 7C), supporting the previous report of this for mitochondria from *rug* lines (Kühn et al., 2011). Ndufs4 is a complex I subunit that is proposed to be present in the peripheral portion of complex I (Klodmann et al., 2010; Klodmann and Braun, 2011). Notably, Nad9, a mitochondrial encoded complex I component, present in the matrix arm, Q module (Klodmann et al., 2010; Klodmann and Braun, 2011) was also slightly decreased in abundance, in the complex I mutants, though it was surprisingly higher in abundance in the *tim23-2* OE line (Figure 7C). A variety of other respiratory chain components increased

Figure 6. (continued).

(A) In vitro uptake assays into mitochondria isolated from Col-0, *tim23-2* OE, and *tim23-2* KO lines. Import of [³⁵S]Met-radiolabeled AOX, F_{AD} subunit of ATP synthase (F_{AD}), MDHAR, ANT, and Pic into isolated mitochondria. Aliquots were removed at 5-, 10-, 15-, and 20-min time points and treated with Proteinase K. The precursor (p) and mature (m) form are indicated.

(B) As in **(A)** except mitochondria were isolated from the *rug* mutant.

(C) As in **(A)** except mitochondria were isolated from complex I mutants *ndufs4* and *rpotmp* lines and imports performed using AOX, MDHAR, and Pic as described above except that 3-, 6-, and 12-min time points were used. All import assays were carried using 50 μ g of isolated mitochondria as determined by protein assay prior to import. The rate of import of the Proteinase K-protected proteins was determined at all time points and normalized to Col-0 (wild-type) at the highest time point for each replicate experiment ($n \geq 3 \pm \text{SE}$).

[See online article for color version of this figure.]

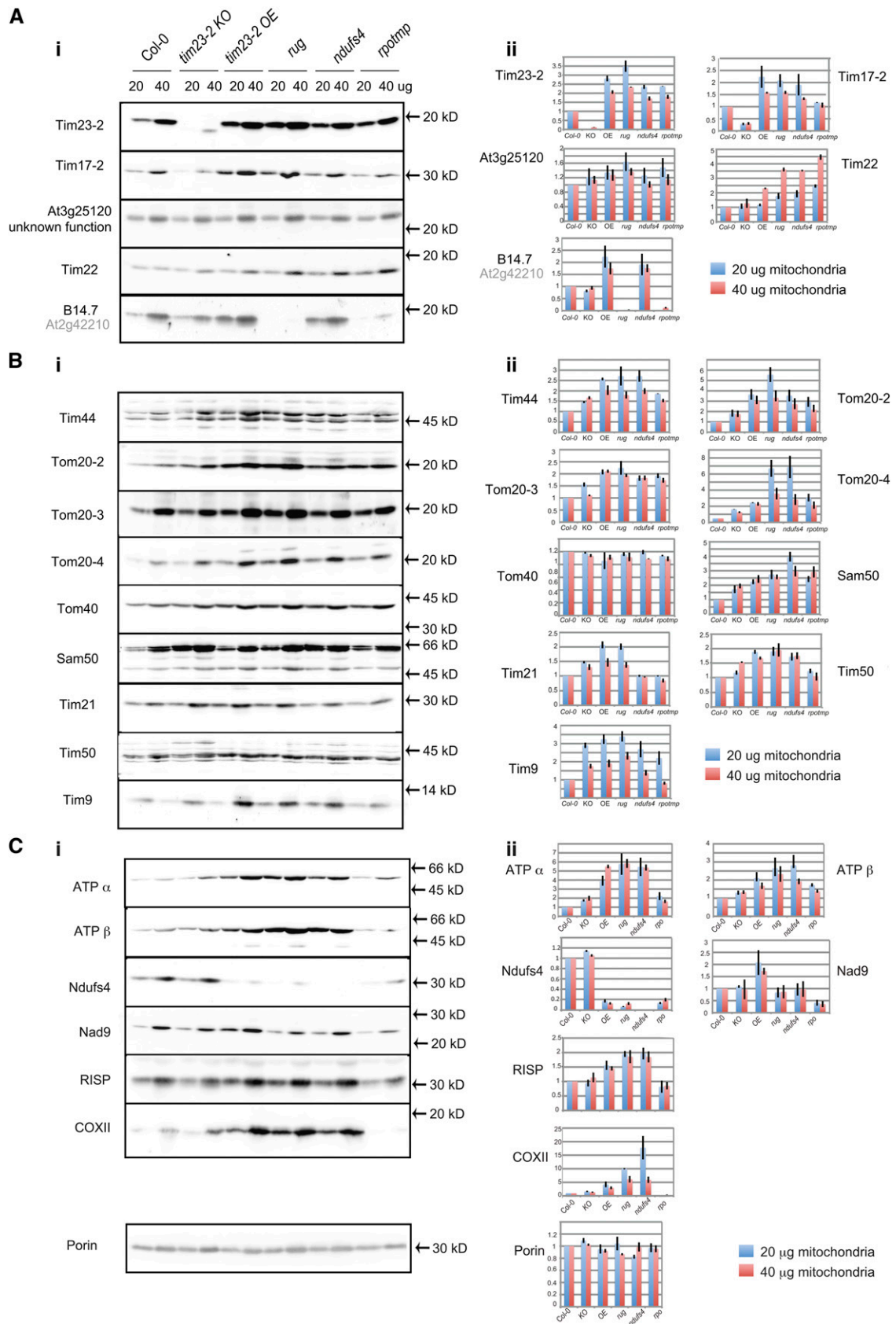


Figure 7. The Abundance of a Variety of Proteins as Determined by Immunoblot Analysis of Mitochondria Isolated from Col-0 (Wild Type), *tim23-2* OE, *tim23-2* KO, and *rug*, *ndufs4*, and *rpotmp* Lines.

in abundance to some extent across the *tim23-2* KO, *tim23-2* OE, and complex I mutant lines, while the α - and β -subunits of the ATP synthase complex increased in abundance most prominently in the *tim23-2* OE, *rug*, and *ndufs4* lines (Figure 7C). COXII protein levels similarly increased in these lines, with barely detectable amounts observed in *rpotmp* (Figure 7C). The Rieske FeS protein of the cytochrome bc₁ complex showed a similar increase in the *tim23-2* OE, *rug*, and *ndufs4* lines (with no increase in the *rpotmp* line) (Figure 7C). Equal loading of total mitochondrial proteins was confirmed with Coomassie blue staining of mitochondrial samples (see Supplemental Figure 5B online), and no changes were observed in the abundance of porin and TOM40 (Figures 7B and 7C). *t* tests and calculation of coefficients of variation (CV) showed no significant ($P < 0.05$) changes and very low variability in protein abundance for both porin (CV < 0.1) and TOM40 (CV < 0.1), confirming equal total mitochondrial protein loading.

Analysis of Global Transcriptional Changes in *Tim23-2* Mutant Plants

tim23-2 OE lines displayed extensive transcriptional reprogramming, with a total of 1645 transcripts significantly altered with respect to Col-0 seedlings (861 transcripts upregulated and 784 transcripts downregulated >1.5-fold, after false discovery rate [FDR] correction [$P < 0.05$, posterior probability of differential expression (PPDE) ($<P > 0.95$)] (Figure 8A). *tim23-2* KO lines displayed fewer significant changes, with 525 and 466 transcripts significantly down- and upregulated >1.5-fold, respectively, after FDR correction. Comparison of transcript responses between the *tim23-2* OE and the complex I mutant *rug* lines showed significant overlap, not only in the specific genes altered, but also the direction and magnitude of the responses. Significantly more transcripts were coexpressed between *rug* and *tim23-2* OE than would be expected by random chance, ($P < 0.001$, χ^2 test) (indicated by #, Figure 8A). This indicates that the transcriptional responses of *rug* and *tim23-2* OE show significant similarity on a genome-wide scale. Transcript abundance changes for components specifically related to mitochondrial import functions were examined in the two mutant lines. For both lines, transcripts encoding mitochondrial intermembrane space chaperones and factors associated with folding in the matrix were consistently upregulated (see Supplemental Table 1 online; Figure 8B).

To investigate further the transcriptomic changes in the *tim23-2* OE mutants in relation to mitochondrial function and regulation, significant differential expression was visualized on a custom

MapMan image, displaying diverse facets of mitochondrial function and biogenesis (Figure 8B). Overexpression of *Tim23-2*, and the associated complex I defect, appears to induce a substantial response within the mitochondrion, including the upregulation of numerous nucleus-encoded and organelle-encoded components of all five cytochrome respiratory pathway complexes (Figure 8B). This is accompanied by an upregulation, at the transcript level, of nuclear-encoded mitochondrial transcription/translation machinery, mitochondrial import components, and a specific upregulation of reactive oxygen species/REDOX scavenging systems within the mitochondria, most likely due to an increase in potential for reactive oxygen species production, due to respiratory chain dysfunction (Figure 7C). Furthermore, steady state mitochondrial encoded transcript levels were measured by quantitative RT-PCR, and a fourfold to 10-fold increase was observed for almost all transcripts encoded by the mitochondrial genome (Figures 8B and 8C). This increase in mitochondrial transcription was also accompanied by an increase in the rates of mitochondrial translation, evident for a number of mitochondrial encoded proteins (Figure 8D). Together, these results suggest that overexpression of *Tim23-2* protein results in the instability of mitochondrial respiratory chain complex I and signals a mitochondrial biogenesis response to induce transcription/translation of all components necessary to build a functional organelle.

This potential regulation of *Tim23-2* with mitochondrial biogenesis is further supported by genome-wide analysis of the coexpression environment of *Tim23-2*. The top 50 coexpressed *Arabidopsis* genes with *Tim23-2* (based on *r* values across >300 public microarray data sets) from the BAR expression Angler and ACT (<http://www.Arabidopsis.leeds.ac.uk/act/coexpanalyser.php>) were combined, leaving a list of 76 unique genes (see Supplemental Table 2 online). Figure 8D shows a functional categorization of this list, compared with the whole genome, and genes are significantly ($P < 0.0001$) overrepresented in the functional categories of protein synthesis (15.8% versus 2.6%), development (11.8% versus 2.8%), protein targeting (6.6% versus 1.1%), RNA binding (6.6% versus 0.7%), RNA processing (6.6% versus 1.1%), cell division (2.6% versus 0.4%), and protein folding (2.6% versus 0.3%), supporting a potential role for *Tim23-2* during mitochondrial biogenesis.

DISCUSSION

The results presented indicate that there is an interaction between complex I of the respiratory chain and TIM17:23 in *Arabidopsis*. It

Figure 7. (continued).

(A) PRAT family members: Immunodetection with antibodies raised against various proteins that belong to the mitochondrial PRAT family. Note that B14.7 is classified as being a member of the PRAT family (Rassow et al., 1999) and a subunit of complex I (Meyer et al., 2008; Klodmann et al., 2010). The protein encoded by At3g25120 has a yet unknown function.

(B) Immunodetection with antibodies to known mitochondrial protein import components.

(C) Immunodetection assays were also completed with antibodies raised against various respiratory chain components representing each complex. Porin was used as a loading control for total protein abundance. Graphs to the right represent the average relative abundance ratios of proteins present in each mutant compared with Col-0 at 20 μ g (blue bar graph) and 40 μ g (red bar graph) of total mitochondrial protein ($n \geq 3 \pm$ se). Standard errors for these average ratios are indicated on each graph.

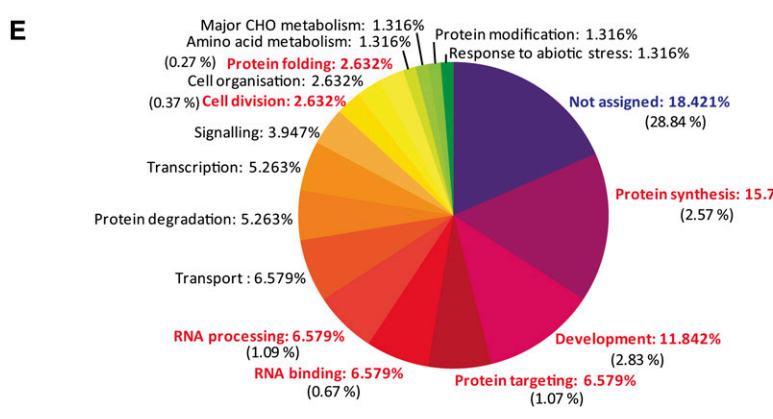
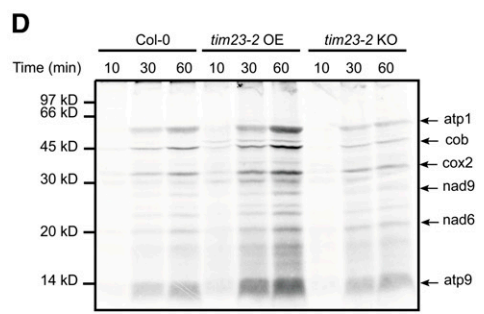
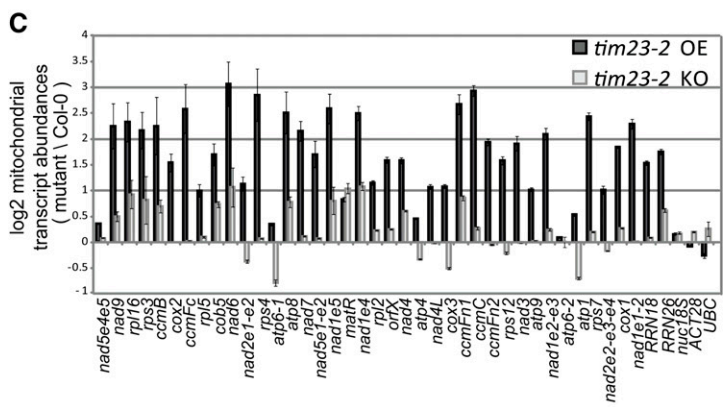
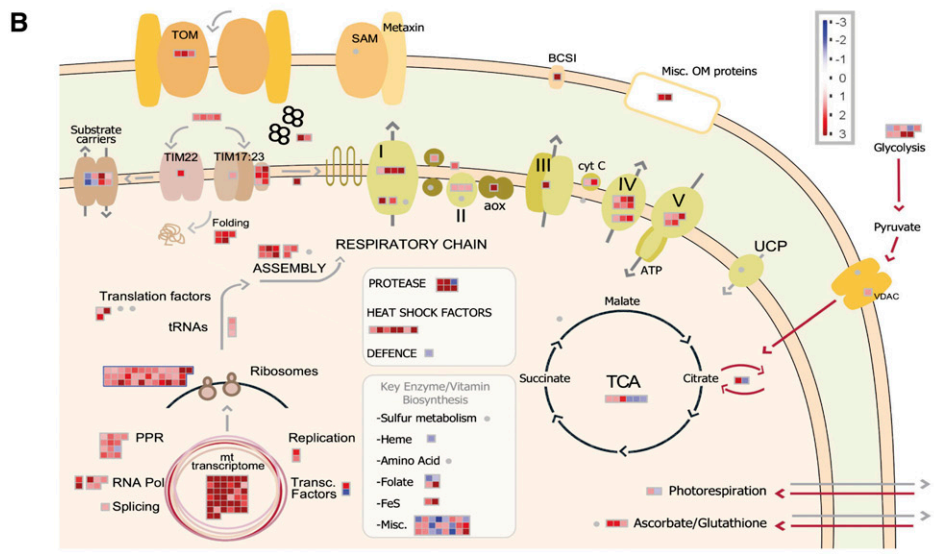
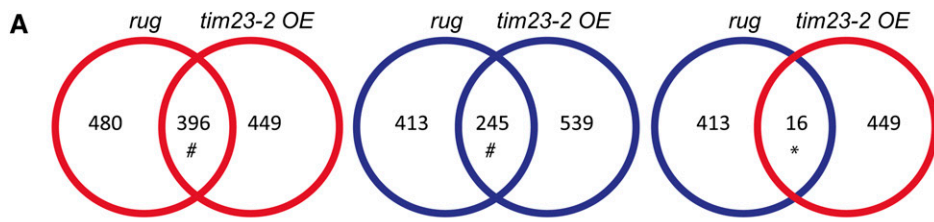


Figure 8. Global Analysis of Transcript Abundance Changes in *tim23-2* OE and KO Lines with Other Mutants Affecting Complex I.

appears that Tim23-2 and B14.7 proteins are both imported into and accumulate in the respiratory complex I and the TIM17:23 complex. Whereas previous studies in yeast have shown interactions between the respiratory chain and protein import complexes, this study reveals an interaction between the protein import components and complex I. It is likely that this interaction was not previously detected simply due to the fact that yeast lack complex I (Melo et al., 2004). In an attempt to investigate further the biological significance of Tim23-2 and B14.7 being present in both complexes, T-DNA insertion lines were screened for B14.7 and Tim23-2. Two homozygous T-DNA insertion lines for Tim23-2 were obtained, and despite repeated self-pollination of heterozygous plants, no homozygous lines for B14.7 could be obtained. For the Tim23-2 T-DNA insertion lines, one line produced TIM23-2 OE plants, while the other line produced authentic KO plants.

None of the other Tim23 isoforms (i.e., Tim23-1 or Tim23-3) were detected in the *tim23-2* KO plants, suggesting that the reason this T-DNA KO was not lethal was because B14.7 could at least partially fulfill the role of Tim23-2. Note that although the *tim23-2* KO plants were viable, a reduced rate of protein import via the general import pathway was seen, indicating that B14.7 could not completely complement the function of Tim23-2. However, a reduced rate of import appears to have no deleterious effect on the growth phenotype; in fact, *tim23-2* KO plants even grew slightly better than Col-0 (Figure 5). It is notable that while Tim23-2 and B14.7 proteins do not display high levels of sequence identity (20 and 33%, respectively), this is not an indication that complementation cannot occur. For example, while Tim23 and Tim17 from yeast and plants do not display high levels of sequence identity, the plant genes for these components can still complement yeast deletion strains and restore viability (Murcha et al., 2007), and B14.7 does have a consensus PRAT domain, whereas Tim23-2 does not (Rassow et al., 1999). Finally even low levels of B14.7 are sufficient to maintain viability, as observed in the *rug* and *rpotmp* KO lines, where only low levels of B14.7 are observed (Figure 7A) (Kühn et al., 2009, 2011). The amount of the TIM23 complex is quite low compared with respiratory chain complexes, even in yeast, where genetic approaches had to be used to characterize TIM translocases,

compared with the more abundant TOM components, which could be characterized by biochemical approaches (Rehling et al., 2001).

Given the nature of this *tim23-2* OE line in *Arabidopsis*, it was not possible to complement this mutant, and previous attempts to overexpress *Tim23-2* using the 35S cauliflower mosaic virus promoter have proved unsuccessful. Therefore, to verify the findings that an increase in Tim23-2 protein abundance resulted in a reduction of complex I, we investigated a number of additional mutants that also exhibit a reduction in complex I activity, including the complex I *rug* mutant, a *nad2* splicing mutant (Kühn et al., 2011), the *rpotmp* mutant (Kühn et al., 2009), and the *ndufs4* mutant (Meyer et al., 2009). In all cases, a reduction in complex I activity resulted in significantly increased Tim23-2 protein abundance. Collectively, these results show that the amounts of complex I and Tim23-2 protein abundance appear to be linked in *Arabidopsis*. Although the link between the amount of complex I and Tim17:23 was unexpected, it is likely that this occurs given that these two complexes share two proteins. Therefore, a mutation that affects complex I assembly, but not the amount of B14.7 directly, may result in additional B14.7 protein being available for assembly into TIM17:23, to replace Tim23-2. In this case, it is proposed that the other subunits of the TIM17:23 complex, which were observed to increase in abundance, compensate to assemble all of the available Tim23-2. However, in *tim23-2* OE plants, it appears that this leads to instability of complex I. The mechanism by which this occurs is unclear but may be explained by the fact that B14.7 is predicted to be on the periphery of complex I (Klodmann et al., 2010; Klodmann and Braun, 2011). Thus, an interaction between complex I and Tim17:23, and Tim17:23 and complex III may facilitate the formation of a supercomplex of complex I+III, which is routinely observed in plant mitochondria (Meyer et al., 2008; Klodmann et al., 2011). However, in the presence of excess Tim23-2, the dynamics of this interaction or equilibrium are altered, leading to instability of complex I (Figure 4). Note that in the *tim23* OE plants, a new complex (MIC) is observed, and this complex is not an assembly intermediate or degradation product of complex I, as analysis of this complex reveals that it contains a variety of proteins (see Supplemental Figure 4 online).

Figure 8. (continued).

(A) Venn diagrams showing the overlap of significantly changing genes at a fold change cutoff of 1.5-fold for *rug* mutants (Kühn et al., 2011) and *tim23-2* OE lines. Red indicates induced transcripts and blue indicates downregulated transcripts.

(B) Overview of significant changes (FDR-corrected $P < 0.05$) in transcript abundance, in response to overexpression of Tim23-2, for transcripts associated with mitochondrial function and organelle biogenesis. Red boxes indicate transcripts that are induced in *tim23-2* OE lines, and blue boxes show transcripts that are downregulated. Color scale is shown as \log_2 fold change.

(C) Quantitative RT-PCR was performed to compare the abundances of mitochondrial transcripts in *tim23-2* OE and KO seedlings compared with Col-0 seedlings. Transcript levels are depicted as \log_2 of the ratio of values determined in mutant versus Col-0 samples for each transcript on the mitochondrial genome. Three technical replicates of three independent biological repeats were performed and averaged per genotype; standard errors are indicated. *Nuclear 18S* (used as a normalization control) along with *ACT2* and *UBC* transcripts were included as controls.

(D) In organellar translations in mitochondria isolated from Col-0, *tim23-2* OE, and KO lines. Equal amounts of mitochondria were used in assays and the incorporation of [35 S]Met was monitored in proteins over time.

(E) The 76 genes defined as highly coexpressed with *tim23-2* were categorized according to function to determine over- or underrepresented groups compared with the whole genome. Categories shown in bold red and blue indicate significantly ($P < 0.0001$, χ^2 test) over- and underrepresented categories, respectively, compared with the whole genome. Percentages shown in parentheses indicate the relevant percentage observed for a whole genome categorization (see Supplemental Tables 1 and 2 online).

We propose that this MIC complex results from the increased expression of a large variety of mitochondrial proteins that are imported but not assembled into functional complexes. To our knowledge, nonassembled proteins have not previously been detected in chemical amounts in mitochondrial complexes that contain several diverse proteins.

The increased abundance of Tim23-2 protein in the *tim23-2* OE line was accompanied by additional changes that together can be grouped into the process of mitochondrial biogenesis. It was notable that transcripts encoding many of the components of the mitochondrial respiratory chain were significantly upregulated in abundance in the *tim23-2* OE line (Figure 8). An analysis of a variety of transcriptome data sets also reveals that this upregulation of respiratory chain components is quite unique (Giraud et al., 2012), as generally transcripts encoding respiratory chain components are stable under a variety of stresses (Clifton et al., 2005) or even in KO of complex I components (Meyer et al., 2009). Furthermore, there are two additional features of the *tim23-2* OE plants that are worth noting: First, a comparison of the protein changes observed with quantitative immunoblotting reveals that the increase in Tom20-2, Tom20-3, and Tom20-4 at a protein level is not accompanied by an increase in the transcript abundance of genes encoding these proteins. This suggests that the protein abundance is regulated at a posttranscriptional level. In a previous study, when any one or two of the Tom20 isoforms in *Arabidopsis* were inactivated, an increase in the other isoforms was observed, again without any change in transcript abundance (Lister et al., 2007), and consistent with posttranscriptional regulation of protein abundance for these components. Similarly, the increase of Tim23-2 protein abundance in the *tim23* OE plants also appears to occur at a posttranscriptional level, supporting the findings from several previous studies indicating that the abundance of mitochondrial protein import components occurs posttranscriptionally (Howell et al., 2006, 2007; Law et al., 2012). The insertion of the T-DNA in the 5' untranslated region may alter translation of *Tim23-2* mRNA, leading to the increase in protein abundance observed in this study. Studies in several plants have revealed a role for the 5' untranslated region in determining translation efficiency (Kawaguchi and Bailey-Serres, 2005; Wever et al., 2010).

Note that examining genes located in close proximity to Tim23-2 from microarray data revealed that transcript abundance for these genes were largely unaffected. Second, while there is a significant overlap in the transcriptome response between the *tim23-2* OE line and the complex I mutant *rug* line, there are also responses that are unique to both (Figure 8A). The response to both mutations displays common features, such as a large reduction in complex I activity, an increase in Tim23-2 abundance and the abundance of various other proteins of the protein import apparatus, and many common changes in the transcriptome. However, differences were also apparent, including the finding that mitochondria from the complex I *rug* mutant also displays an increase in the rate of protein imported via the carrier import pathway and transcripts encoding components of the mitochondrial respiratory chain are not upregulated in this mutant. Finally, the overexpression of yeast Tim23 in yeast cells using the galactose promoter to drive expression

resulted in no detrimental effects (Emtage and Jensen, 1993; Bauer et al., 1996), unlike what we have seen for plants in this study. It is proposed that the difference between plants (and likely other organisms, such as yeast) may be due to the fact that mitochondrial biogenesis and respiratory chain activity in yeast are not linked, given that yeast is a facultative anaerobic organism. Thus, it is not surprising that the expression of the respiratory chain components and mitochondrial biogenesis are not coupled. Rather, in yeast, the expression of mitochondrial respiratory chain components is under the control of heme-activated proteins that are in turn regulated by the availability of oxygen (Kwast et al., 1998). However, mitochondrial biogenesis still occurs in the absence of oxygen; thus, the respiratory chain and mitochondrial biogenesis are not coupled in yeast. By contrast, respiratory chain activity and mitochondrial biogenesis may be linked in multicellular organisms. Thus, the interaction reported in this study, between complex I and TIM17:23 in *Arabidopsis*, provides a mechanism to link mitochondrial biogenesis and activity.

In conclusion, the results presented here show that in *Arabidopsis*, the B14.7 and Tim23-2 proteins are imported into and accumulate in two mitochondrial protein complexes: the respiratory chain complex I and the protein import complex TIM17:23. It is also seen that the abundance of complex I is inversely related to the abundance of Tim23. This may provide for an elegant system to regulate mitochondrial biogenesis, as any changes in complex I, due to oxidative damage or increased respiratory demand, could trigger signals that increase the amount of Tim23-2 protein and thus activate mitochondrial biogenesis.

METHODS

Gene Identification and Phylogenetic Analysis of Proteins

The Mitochondrial Protein Import Components database (Lister et al., 2003) and The Arabidopsis Information Resource (www.Arabidopsis.org) was used to identify genes used in this study. Alignments were performed using ClustalW2 (www.ebi.ac.uk).

Plant Material and Culture Conditions

The SALK T-DNA insertion lines were obtained from the ABRC seed stock center (Alonso et al., 2003), and GABI lines were obtained from GABI-Kat (Rosso et al., 2003) for Tim23-2 (SALK_143656 and GABI_689C11). Lines were screened for homozygosity of the T-DNA insert with primers listed in Supplemental Table 3 online, as previously outlined (Carrie et al., 2010b; Kühn et al., 2011). T-DNA mutants and the wild type were germinated on 0.5× Gamborg's B5 salt medium containing 3% (w/v) Suc grown at 22°C with a light intensity of 80 $\mu\text{mol quanta m}^{-2} \text{s}^{-1}$ in a 16-h photoperiod.

DNA and PCR

Genomic DNA was isolated from 14-d-old plants, and PCR was performed using the REExtract-N-Amp Plant PCR kit (Sigma-Aldrich) according to the manufacturer's instructions. Cloning from cDNA was performed as previously described (Murcha et al., 2003) using primers listed in Supplemental Table 3 online.

Isolation of Mitochondria from *Arabidopsis thaliana* Plants

For the isolation of mitochondria from water-cultured plants, mutant and Col-0 seeds were sterilized and inoculated in half-strength Murashige and

Skoog media, containing 0.5× Gamborg's B5 salts, 3% (w/v) Suc, 50 µg/ml cefotaxime, and 2 mM MES KOH, pH 5.7. Plants were grown for 2 weeks as described above and mitochondria isolated as described previously (Lister et al., 2007).

BN-PAGE and Immunodetection of Protein Complexes

BN-PAGE was performed according to Jänsch et al. (1996) as described by Meyer et al. (2009). Following separation, gels were stained with Coomassie Brilliant Blue, subjected to an in-gel complex I activity assay, or transferred to polyvinylidene difluoride membrane and immunodetected with a selection of antibodies as described below.

In-Gel Complex I Activity Assay

The assay was performed according to Zerbetto et al. (1997).

Immunoblot Analysis

Mitochondrial protein was separated by SDS-PAGE and transferred to Hybond-C extra nitrocellulose membrane (GE Healthcare). Immunodetection of proteins was performed as described previously (Murcha et al., 2005a). The linearity of the response of the antibodies were tested with 10, 20, and 40 µg of mitochondrial proteins (see Supplemental Figure 5A online) and equal protein loading confirmed by staining with Coomassie Brilliant Blue (see Supplemental Figure 5B online). Furthermore, the CV was calculated for fold changes in abundances of porin and Tom40 to ensure that they were of equal abundance in samples. The CV was determined by calculating the ratio of the standard deviation of the mean, providing a statistical indication of the spread/variation in abundance. Antibodies used were raised against Tim17-2 (Murcha et al., 2005a), Tom20-2, 20-3, 20-4, Metaxin (Lister et al., 2007), Tom40, RISP, Sam50 (Carrie et al., 2010b), AOX, α -subunit of ATP synthase, Porin (Elthon et al., 1989), Nad9 (Lamattina et al., 1993), COXII, cytochrome c, β -subunit of ATP synthase (Agrisera), and Ndufs4 (Meyer et al., 2009). For the remaining antibodies, recombinant proteins of Tim9 (At3g46560, amino acids 1 to 93), Tim50 (At1g55900, amino acids 110 to 269), Tim44 (At2g36070, amino acids 100 to 472), Tim21 (At4g00026, amino acids 160 to 376), Tim23-2 (At1g72750, amino acids 3 to 32 and 103 to 143), Tim23-3 (At3g04800, amino acids 6 to 32 and 64 to 132), At3g25120 (amino acids, amino acids 89 to 189), were expressed and purified as previously outlined (Carrie et al., 2010b). For antibodies raised against B14.7 (At2g42210) (amino acids 1 to 100) and Tim22 (At3g10110/At1g18320 amino acids 1 to 50), cDNA was cloned into pDest15 using Gateway technology, and glutathione S-transferase-tagged recombinant proteins were expressed, bound to GST-Sepharose (Scientifix), and electroeluted. Recombinant proteins were confirmed by mass spectrometry prior to inoculation into rabbits as per the standard protocol (Cooper and Paterson, 2008). Immunodetection of newly synthesized antibodies was performed at a 1 in 5000 dilution against purified mitochondria.

In Vitro Import Studies

Mitochondria for in vitro import experiments were prepared from 14-d-old *Arabidopsis* seedlings grown in liquid culture, as previously described (Lister et al., 2007). [³⁵S]Met-labeled precursor proteins of AOX (X68702) (Whelan et al., 1995), F₁d subunit of ATP synthase (X74296) (Smith et al., 1994), ANT (X57556), Pic (AB016063) (Murcha et al., 2005a), and MDHAR (At3g09940) (Chew et al., 2003) synthesized using the rabbit reticulocyte T_NT in vitro transcription/translation lysate (Promega). Import of radio-labeled precursor protein into isolated mitochondria was performed as previously described (Lister et al., 2007) at increasing time points. Following import, mitochondria were pelleted at 20,000g for 5 min and subjected to SDS-PAGE analysis. Gels were stained in Coomassie

Brilliant Blue, dried, and exposed to a BAS TR2040 phosphor-imaging plate (Fuji) for 24 h. The exposed plate was visualized using the BAS 2500 Bio-Imaging Analyzer (Fuji). Proteinase K-protected, mature, radiolabeled imported proteins were quantified at each time point and normalized to the highest time point for the wild type, which was set to 1 using Quantity One software (Bio-Rad) (Lister et al., 2007). Three biological replicates were performed for each mutant and precursor protein and the average (and se) of import amount relative to Col-0 was determined.

Imports analyzed by BN-PAGE were performed as previously described (Carrie et al., 2010b). [³⁵S]Met-labeled precursor proteins of Tim17-2 (At2g37410), Tim23-2 (At1g72750) (Murcha et al., 2005a), Tim21 (At4g00026), complex I subunit At1g4726, MPP α (At1g51980) (Kühn et al., 2011), B14.7 complex I subunit At2g42210 (Murcha et al., 2007), and cytochrome c, subunit of ubiquinone cytochrome c reductase (At4g32470) were generated from *Arabidopsis* cDNA cloned into pDest14 using Gateway technology (Invitrogen) and used in import assays. Precursor proteins were synthesized and imported as described previously except that 250 µg of mitochondrial protein was used per time point. Following import, mitochondria were pelleted at 20,000g for 5 min and subjected to BN-PAGE analysis as detailed above. BN-PAGE gels were fixed in 40% (v/v) methanol and 10% (v/v) acetic acid and visualized by autoradiography, as described above.

RNA Isolation and Global Transcript Analysis

Analysis of the changes in transcript abundance between Col-0, *tim23-2 OE*, and *tim23-2 KO* lines was performed using Affymetrix GeneChip *Arabidopsis* ATH1 Genome Arrays (Affymetrix). Whole rosettes from several seedlings at the 8 true leaf stage of development, grown under a 16-h photoperiod, were pooled for each biological replicate. Col-0 and mutant tissue samples were collected in biological triplicate. For each replicate, total RNA was isolated and microarrays were performed as described (Kühn et al., 2011).

Quantitative RT-PCR

RNA, isolated as described above, from Col-0, *tim23-2 OE*, and *tim23-2 KO* plants was subjected to two consecutive treatments with TURBO DNase (Ambion), confirmed by PCR to be free of detectable amounts of DNA, and reverse transcribed exactly as described (Kühn et al., 2009). Quantitative RT-PCR on the mitochondrial transcriptome was performed using the LightCycler 480 SYBR Green I Master Mix (Roche Applied Science) using the PCR program and primer pairs and analyzed as described (Kühn et al., 2009).

Statistical Analysis of Microarray Data

Data quality was assessed using GCOS 1.4 before CEL files were exported into AVADIS Prophetic (version 4.3; Strand Genomics) and Partek Genomics Suite software, version 6.3, for further analysis. CEL files are available at Array Express (<http://www.ebi.ac.uk/arrayexpress/>) under the accession number E-MEXP-3309. Public array data for the *rug* mutant (Kühn et al., 2011) was also independently analyzed and included. MAS5 normalization algorithms were performed only to generate present/absent calls across the arrays. Probe sets that recorded absent calls in two or more of the three biological replicates for all four genotypes conditions were removed from further analysis. Bacterial controls, probe sets for organelle transcripts and ambiguous probe sets for multiple transcripts were also removed, resulting in a final set of 14,831 probe identifiers for downstream analysis. CEL files were also subjected to GC content background robust multiarray average normalization for computing fluorescence intensity values used in differential expression analyses. Correlation plots were examined between all arrays using the scatterplot

function in the Partek Genomics Suite, and in all cases $r > 0.98$ (data not shown). Analysis of differential expression was performed using a regularized t test based on a Bayesian statistical framework using the software program Cyber-T (Baldi and Long, 2001) (<http://cybert.microarray.ics.uci.edu/>). Cyber-T employs a mixture model-based method described by Allison et al. (2006) for the computation of the global false-positive and false-negative levels inherent in a DNA microarray experiment. To control for FDR accurately and minimize false positives within the differential expression analysis, PPDE(P) values and PPDE(>P) values were calculated, as a means to measure the true discovery rate ($1 - \text{FDR}$). Changes in transcript abundance were considered significant with a PPDE(>P) > 0.95 and a fold change > 1.5 -fold. Overlaps in the transcript abundance responses for the different genotypes were plotted on Venn diagrams to determine statistically significant over- or underrepresentation in the overlap, compared with that which is expected by random chance, using a Pearson's χ^2 test for independence. Transcript abundance changes for mitochondrial proteins were visualized in a custom MapMan pathway (Thimm et al., 2004). A nonredundant list of 76 transcripts that are the most highly coexpressed transcripts, genome wide, against *Tim23-2* was created from the top 50 gene hits from BAR Expression Angler and The Arabidopsis Coexpression Data Mining Tools (coexpression multi-experiment tool, <http://www.Arabidopsis.leeds.ac.uk/act/coexpanalyser.php#CO2>) shown in Supplemental Table 2 online (Manfield et al., 2006). Cocorrelation scatterplots were generated using the cocorrelation 2-D Pearson correlation coefficients plot, with the 76 coexpressed top hit transcripts highlighted. Functional categorization analysis was performed using simplified annotation categories defined in MapMan software bins to define over/underrepresented functional groups based on percentile distributions of the whole genome.

In Organello Protein Synthesis Assays

Mitochondria were isolated as described above and protein synthesis reactions were performed as previously described (Giegé et al., 2005).

Yeast Two-Hybrid Protein Interactions

Yeast two-hybrid interaction assays were performed as described (Giraud et al., 2010). AH109 cells transformed with pGAD *Tim23-2* were mated with Y187 cells transformed with pGBK *Tim17-2*, pGBK *Tim23-2*, pGBK *Tim50*, pGBK B14.7, pGBK *Tim21*, pGBK MPP α , and empty pGBK. Serial dilutions of yeast growing on auxotrophic selection media (–Leu –Trp –His –Ade) were regrown on selection plates for diploid selection (–Trp –Leu) and positive interaction selection (–Trp –Leu –Ade –His and –Leu –Trp –Ade –His with X- α -D-galactoside).

Immunoprecipitations

Two hundred micrograms of mitochondria was solubilized in digitonin buffer consisting of 30 mM HEPES KOH, pH 7.4, 150 mM potassium acetate, 10% (v/v) glycerol, and 1 mg digitonin and placed on ice for 20 min. One hundred microliters of Protein A Sepharose with or without 10 μ L of antibody was added with solubilization buffer without digitonin, including 0.5% (w/v) BSA and Complete Protease inhibitor (Roche), and incubated for 3 h at 4°C. Beads were washed and samples resolved by SDS-PAGE, transferred to nitrocellulose membrane, and immunodetected with antibodies indicated.

BiFC

BiFC was performed as outlined previously (Citovsky et al., 2008) in onion (*Allium cepa*) epidermal cells. Images were captured using Cell imaging software (Olympus) as previously described (Carrie et al., 2009).

Blue Native Elution and in-Gel Digestion

The complex of interest was excised from Blue native gels and proteins extracted by electroelution. Gel slices were minced by passing back and forth between two syringes and added to the H-shaped eluter vessel of a CBS Scientific electroeluter. Proteins were eluted according to the technique detailed previously (Hunkapiller et al., 1983). Protein identification was performed by in-gel digestion and electrospray ionization tandem mass spectrometry according to previous methods (Meyer et al., 2007).

Accession Numbers

Sequence data from this article can be found in the Arabidopsis Genome Initiative or GenBank/EMBL databases under the following accession numbers: *Tim17-1* (At1g20350), *Tim17-2* (At2g37410), *Tim17-3* (At5g11690), *Tim23-1* (At1g17530), *Tim23-2* (At1g72750), *Tim23-3* (At3g04800), B14.7 (At2g42210), MPP α (At3g16480), *Tim50* (At1g55900), *Ndufs4* (At5g67590), *RISP* (At5g13430), *COXII* (AtMg00160), α -ATP synthase (At2g07698), *rug* (At5g60870), *Rpotmp* (At5g15700), *Tim22* (At1g18320/At3g10110), *Tim44* (At2g36070), *Tom20-2* (At1g27390), *Tom20-3* (At3g27080), *Tom20-4* (At5g40930), *Sam50* (At5g05520), *Tim21* (At4g00026), *Tim9* (At3g46560), *Tom40* (At3g20000), *cyc1-1* (At3g27240), and *cyc1-2* (At5g40810).

Supplemental Data

The following materials are available in the online version of this article.

Supplemental Figure 1. Determining the Specificity of B14.7 Antibody.

Supplemental Figure 2. Interaction of *Tim21* with Complex III in *Arabidopsis*.

Supplemental Figure 3. Analysis of *Tim23* Protein and Transcript Abundance in T-DNA Insertion Lines.

Supplemental Figure 4. Identification of the Mixed Inner Membrane Complex in the *tim23-2* OE Line.

Supplemental Figure 5. Determining the Linearity of Antibodies Used and Protein Abundance in Mitochondrial Isolations.

Supplemental Table 1. Summary of Changes in Transcript Abundance for Nuclear Genes Encoding Mitochondrial Import and Assembly Components.

Supplemental Table 2. Summary of 76 Transcripts Defined as Being Highly Coexpressed with *tim23-2* across Public *Arabidopsis* Microarray Data Sets.

Supplemental Table 3. List of Primers Used in This Study.

ACKNOWLEDGMENTS

This work was supported by the University of Western Australia Scholarship for International Research Fees grant to Y.W., an Australian Research Council Australian Postdoctoral Fellowship grant to M.W.M., and the Australian Research Council Centre of Excellence Program CEO561495.

AUTHOR CONTRIBUTIONS

J.W. and M.W.M. designed the experiments and wrote the article. Y.W., C.C., D.E., O.D., and M.W.M. performed the experimental procedures and carried out the data analysis. E.G. and R.N. carried out gene expression and transcriptome analysis.

Received March 27, 2012; revised May 22, 2012; accepted June 11, 2012; published June 22, 2012.

REFERENCES

- Allison, D.B., Cui, X., Page, G.P., and Sabripour, M. (2006). Microarray data analysis: From disarray to consolidation and consensus. *Nat. Rev. Genet.* **7**: 55–65.
- Alonso, J.M. et al. (2003). Genome-wide insertional mutagenesis of *Arabidopsis thaliana*. *Science* **301**: 653–657.
- Baldi, P., and Long, A.D. (2001). A Bayesian framework for the analysis of microarray expression data: Regularized t-test and statistical inferences of gene changes. *Bioinformatics* **17**: 509–519.
- Bauer, M.F., Sirrenberg, C., Neupert, W., and Brunner, M. (1996). Role of Tim23 as voltage sensor and presequence receptor in protein import into mitochondria. *Cell* **87**: 33–41.
- Boyes, D.C., Zayed, A.M., Ascenzi, R., McCaskill, A.J., Hoffman, N.E., Davis, K.R., and Görlach, J. (2001). Growth stage-based phenotypic analysis of *Arabidopsis*: A model for high throughput functional genomics in plants. *Plant Cell* **13**: 1499–1510.
- Braun, H.P., Emmermann, M., Kruff, V., and Schmitz, U.K. (1992). The general mitochondrial processing peptidase from potato is an integral part of cytochrome c reductase of the respiratory chain. *EMBO J.* **11**: 3219–3227.
- Brumme, S., Kruff, V., Schmitz, U.K., and Braun, H.P. (1998). New insights into the co-evolution of cytochrome c reductase and the mitochondrial processing peptidase. *J. Biol. Chem.* **273**: 13143–13149.
- Carrie, C., Giraud, E., Duncan, O., Xu, L., Wang, Y., Huang, S., Clifton, R., Murcha, M., Filipovska, A., Rackham, O., Vrielink, A., and Whelan, J. (2010b). Conserved and novel functions for *Arabidopsis thaliana* MIA40 in assembly of proteins in mitochondria and peroxisomes. *J. Biol. Chem.* **285**: 36138–36148.
- Carrie, C., Kühn, K., Murcha, M.W., Duncan, O., Small, I.D., O'Toole, N., and Whelan, J. (2009). Approaches to defining dual-targeted proteins in *Arabidopsis*. *Plant J.* **57**: 1128–1139.
- Carrie, C., Murcha, M.W., and Whelan, J. (2010a). An in silico analysis of the mitochondrial protein import apparatus of plants. *BMC Plant Biol.* **10**: 249.
- Carroll, J., Shannon, R.J., Fearnley, I.M., Walker, J.E., and Hirst, J. (2002). Definition of the nuclear encoded protein composition of bovine heart mitochondrial complex I. Identification of two new subunits. *J. Biol. Chem.* **277**: 50311–50317.
- Chacinska, A., van der Laan, M., Mehnert, C.S., Guiard, B., Mick, D.U., Hutu, D.P., Truscott, K.N., Wiedemann, N., Meisinger, C., Pfanner, N., and Rehling, P. (2010). Distinct forms of mitochondrial TOM-TIM supercomplexes define signal-dependent states of pre-protein sorting. *Mol. Cell. Biol.* **30**: 307–318.
- Chew, O., Whelan, J., and Millar, A.H. (2003). Molecular definition of the ascorbate-glutathione cycle in *Arabidopsis* mitochondria reveals dual targeting of antioxidant defenses in plants. *J. Biol. Chem.* **278**: 46869–46877.
- Citovsky, V., Gafni, Y., and Tzfira, T. (2008). Localizing protein-protein interactions by bimolecular fluorescence complementation in planta. *Methods* **45**: 196–206.
- Clifton, R., Lister, R., Parker, K.L., Sappl, P.G., Elhafez, D., Millar, A.H., Day, D.A., and Whelan, J. (2005). Stress-induced co-expression of alternative respiratory chain components in *Arabidopsis thaliana*. *Plant Mol. Biol.* **58**: 193–212.
- Cooper, H.M., and Paterson, Y. (2008). Production of polyclonal antisera. *Curr. Protoc. Mol. Biol.* **81**: 11.12.1–11.12.10.
- Dekker, P.J., Keil, P., Rassow, J., Maarse, A.C., Pfanner, N., and Meijer, M. (1993). Identification of MIM23, a putative component of the protein import machinery of the mitochondrial inner membrane. *FEBS Lett.* **330**: 66–70.
- Dolezal, P., Likic, V., Tachezy, J., and Lithgow, T. (2006). Evolution of the molecular machines for protein import into mitochondria. *Science* **313**: 314–318.
- Dudkina, N.V., Kouril, R., Peters, K., Braun, H.P., and Boekema, E.J. (2010). Structure and function of mitochondrial super-complexes. *Biochim. Biophys. Acta* **1797**: 664–670.
- Dutilleul, C., Garmier, M., Noctor, G., Mathieu, C., Chétrit, P., Foyer, C.H., and de Paepe, R. (2003). Leaf mitochondria modulate whole cell redox homeostasis, set antioxidant capacity, and determine stress resistance through altered signaling and diurnal regulation. *Plant Cell* **15**: 1212–1226.
- Elthon, T.E., Nickels, R.L., and McIntosh, L. (1989). Monoclonal antibodies to the alternative oxidase of higher plant mitochondria. *Plant Physiol.* **89**: 1311–1317.
- Emtage, J.L., and Jensen, R.E. (1993). MAS6 encodes an essential inner membrane component of the yeast mitochondrial protein import pathway. *J. Cell Biol.* **122**: 1003–1012.
- Eriksson, A.C., Sjöling, S., and Glaser, E. (1996). Characterization of the bifunctional mitochondrial processing peptidase (MPP)/bc1 complex in *Spinacia oleracea*. *J. Bioenerg. Biomembr.* **28**: 285–292.
- Gebert, N. et al. (2011). Dual function of Sdh3 in the respiratory chain and TIM22 protein translocase of the mitochondrial inner membrane. *Mol. Cell* **44**: 811–818.
- Giegé, P., Sweetlove, L.J., Cognat, V., and Leaver, C.J. (2005). Co-ordination of nuclear and mitochondrial genome expression during mitochondrial biogenesis in *Arabidopsis*. *Plant Cell* **17**: 1497–1512.
- Giraud, E., Ng, S., Carrie, C., Duncan, O., Low, J., Lee, C.P., Van Aken, O., Millar, A.H., Murcha, M., and Whelan, J. (2010). TCP transcription factors link the regulation of genes encoding mitochondrial proteins with the circadian clock in *Arabidopsis thaliana*. *Plant Cell* **22**: 3921–3934.
- Giraud, E., Van Aken, O., Uggalla, V., and Whelan, J. (2012). REDOX regulation of mitochondrial function in plants. *Plant Cell Environ.* **35**: 271–280.
- Glaser, E., and Dessi, P. (1999). Integration of the mitochondrial-processing peptidase into the cytochrome bc1 complex in plants. *J. Bioenerg. Biomembr.* **31**: 259–274.
- Glaser, E., Eriksson, A., and Sjöling, S. (1994). Bifunctional role of the bc1 complex in plants. Mitochondrial bc1 complex catalyses both electron transport and protein processing. *FEBS Lett.* **346**: 83–87.
- Hewitt, V., Alcock, F., and Lithgow, T. (2011). Minor modifications and major adaptations: The evolution of molecular machines driving mitochondrial protein import. *Biochim. Biophys. Acta* **1808**: 947–954.
- Howell, K.A., Cheng, K., Murcha, M.W., Jenkin, L.E., Millar, A.H., and Whelan, J. (2007). Oxygen initiation of respiration and mitochondrial biogenesis in rice. *J. Biol. Chem.* **282**: 15619–15631.
- Howell, K.A., Millar, A.H., and Whelan, J. (2006). Ordered assembly of mitochondria during rice germination begins with pro-mitochondrial structures rich in components of the protein import apparatus. *Plant Mol. Biol.* **60**: 201–223.
- Hunkapiller, M.W., Lujan, E., Ostrander, F., and Hood, L.E. (1983). Isolation of microgram quantities of proteins from polyacrylamide gels for amino acid sequence analysis. *Methods Enzymol.* **91**: 227–236.
- Jansch, L., Kruff, V., Schmitz, U.K., and Braun, H.P. (1996). New insights into the composition, molecular mass and stoichiometry of the protein complexes of plant mitochondria. *Plant J.* **9**: 357–368.
- Kawaguchi, R., and Bailey-Serres, J. (2005). mRNA sequence features that contribute to translational regulation in *Arabidopsis*. *Nucleic Acids Res.* **33**: 955–965.
- Klodmann, J., and Braun, H.P. (2011). Proteomic approach to characterize mitochondrial complex I from plants. *Phytochemistry* **72**: 1071–1080.

- Klodmann, J., Senkler, M., Rode, C., and Braun, H.P. (2011). Defining the protein complex proteome of plant mitochondria. *Plant Physiol.* **157**: 587–598.
- Klodmann, J., Sunderhaus, S., Nitz, M., Jansch, L., and Braun, H.P. (2010). Internal architecture of mitochondrial complex I from *Arabidopsis thaliana*. *Plant Cell* **22**: 797–810.
- Kühn, K., Carrie, C., Giraud, E., Wang, Y., Meyer, E.H., Narsai, R., des Francs-Small, C.C., Zhang, B., Murcha, M.W., and Whelan, J. (2011). The RCC1 family protein RUG3 is required for splicing of *nad2* and complex I biogenesis in mitochondria of *Arabidopsis thaliana*. *Plant J.* **67**: 1067–1080.
- Kühn, K., Richter, U., Meyer, E.H., Delannoy, E., de Longevialle, A. F., O'Toole, N., Börner, T., Millar, A.H., Small, I.D., and Whelan, J. (2009). Phage-type RNA polymerase RPOTmp performs gene-specific transcription in mitochondria of *Arabidopsis thaliana*. *Plant Cell* **21**: 2762–2779.
- Kwast, K.E., Burke, P.V., and Poyton, R.O. (1998). Oxygen sensing and the transcriptional regulation of oxygen-responsive genes in yeast. *J. Exp. Biol.* **201**: 1177–1195.
- Lamattina, L., Gonzalez, D., Gualberto, J., and Grienenberger, J.M. (1993). Higher plant mitochondria encode an homologue of the nuclear-encoded 30-kDa subunit of bovine mitochondrial complex I. *Eur. J. Biochem.* **217**: 831–838.
- Law, S.R., Narsai, R., Taylor, N.L., Delannoy, E., Carrie, C., Giraud, E., Millar, A.H., Small, I., and Whelan, J. (2012). Nucleotide and RNA metabolism prime translational initiation in the earliest events of mitochondrial biogenesis during *Arabidopsis* germination. *Plant Physiol.* **158**: 1610–1627.
- Lister, R., Carrie, C., Duncan, O., Ho, L.H., Howell, K.A., Murcha, M.W., and Whelan, J. (2007). Functional definition of outer membrane proteins involved in preprotein import into mitochondria. *Plant Cell* **19**: 3739–3759.
- Lister, R., Murcha, M.W., and Whelan, J. (2003). The Mitochondrial Protein Import Machinery of Plants (MPIIMP) database. *Nucleic Acids Res.* **31**: 325–327.
- Maarse, A.C., Blom, J., Keil, P., Pfanner, N., and Meijer, M. (1994). Identification of the essential yeast protein MIM17, an integral mitochondrial inner membrane protein involved in protein import. *FEBS Lett.* **349**: 215–221.
- Manfield, I.W., Jen, C.H., Pinney, J.W., Michalopoulos, I., Bradford, J.R., Gilmartin, P.M., and Westhead, D.R. (2006). *Arabidopsis* Co-expression Tool (ACT): Web server tools for microarray-based gene expression analysis. *Nucleic Acids Res.* **34** (Web Server issue): W504–W509.
- Melo, A.M., Bandeiras, T.M., and Teixeira, M. (2004). New insights into type II NAD(P)H:quinone oxidoreductases. *Microbiol. Mol. Biol. Rev.* **68**: 603–616.
- Meyer, E.H., Heazlewood, J.L., and Millar, A.H. (2007). Mitochondrial acyl carrier proteins in *Arabidopsis thaliana* are predominantly soluble matrix proteins and none can be confirmed as subunits of respiratory Complex I. *Plant Mol. Biol.* **64**: 319–327.
- Meyer, E.H., Taylor, N.L., and Millar, A.H. (2008). Resolving and identifying protein components of plant mitochondrial respiratory complexes using three dimensions of gel electrophoresis. *J. Proteome Res.* **7**: 786–794.
- Meyer, E.H., Tomaz, T., Carroll, A.J., Estavillo, G., Delannoy, E., Tanz, S.K., Small, I.D., Pogson, B.J., and Millar, A.H. (2009). Remodeled respiration in *ndufs4* with low phosphorylation efficiency suppresses *Arabidopsis* germination and growth and alters control of metabolism at night. *Plant Physiol.* **151**: 603–619.
- Mokranjac, D., and Neupert, W. (2010). The many faces of the mitochondrial TIM23 complex. *Biochim. Biophys. Acta* **1797**: 1045–1054.
- Murcha, M.W., Elhafez, D., Lister, R., Tonti-Filippini, J., Baumgartner, M., Philippar, K., Carrie, C., Mokranjac, D., Soll, J., and Whelan, J. (2007). Characterization of the preprotein and amino acid transporter gene family in *Arabidopsis*. *Plant Physiol.* **143**: 199–212.
- Murcha, M.W., Elhafez, D., Millar, A.H., and Whelan, J. (2005b). The C-terminal region of TIM17 links the outer and inner mitochondrial membranes in *Arabidopsis* and is essential for protein import. *J. Biol. Chem.* **280**: 16476–16483.
- Murcha, M.W., Lister, R., Ho, A.Y., and Whelan, J. (2003). Identification, expression, and import of components 17 and 23 of the inner mitochondrial membrane translocase from *Arabidopsis*. *Plant Physiol.* **131**: 1737–1747.
- Murcha, M.W., Millar, A.H., and Whelan, J. (2005a). The N-terminal cleavable extension of plant carrier proteins is responsible for efficient insertion into the inner mitochondrial membrane. *J. Mol. Biol.* **351**: 16–25.
- Murray, J., Zhang, B., Taylor, S.W., Oglesbee, D., Fahy, E., Marusich, M.F., Ghosh, S.S., and Capaldi, R.A. (2003). The subunit composition of the human NADH dehydrogenase obtained by rapid one-step immunopurification. *J. Biol. Chem.* **278**: 13619–13622.
- Nehls, U., Hemmer, S., Röhlen, D.A., Van der Pas, J.C., Preis, D., Sackmann, U., and Weiss, H. (1991). cDNA and genomic DNA sequence of the 21.3 kDa subunit of NADH:ubiquinone reductase (complex I) from *Neurospora crassa*. *Biochim. Biophys. Acta* **1088**: 325–326.
- Perry, A.J., Hulett, J.M., Likić, V.A., Lithgow, T., and Gooley, P.R. (2006). Convergent evolution of receptors for protein import into mitochondria. *Curr. Biol.* **16**: 221–229.
- Rassow, J., Dekker, P.J., van Wilpe, S., Meijer, M., and Soll, J. (1999). The preprotein translocase of the mitochondrial inner membrane: Function and evolution. *J. Mol. Biol.* **286**: 105–120.
- Rehling, P., Brandner, K., and Pfanner, N. (2004). Mitochondrial import and the twin-pore translocase. *Nat. Rev. Mol. Cell Biol.* **5**: 519–530.
- Rehling, P., Wiedemann, N., Pfanner, N., and Truscott, K.N. (2001). The mitochondrial import machinery for preproteins. *Crit. Rev. Biochem. Mol. Biol.* **36**: 291–336.
- Rode, C., Senkler, M., Klodmann, J., Winkelmann, T., and Braun, H.P. (2011). GelMap—a novel software tool for building and presenting proteome reference maps. *J. Proteomics* **74**: 2214–2219.
- Rosso, M.G., Li, Y., Strizhov, N., Reiss, B., Dekker, K., and Weisshaar, B. (2003). An *Arabidopsis thaliana* T-DNA mutagenized population (GABI-Kat) for flanking sequence tag-based reverse genetics. *Plant Mol. Biol.* **53**: 247–259.
- Schmidt, O., Pfanner, N., and Meisinger, C. (2010). Mitochondrial protein import: From proteomics to functional mechanisms. *Nat. Rev. Mol. Cell Biol.* **11**: 655–667.
- Schulte, U., Arretz, M., Schneider, H., Tropschug, M., Wachter, E., Neupert, W., and Weiss, H. (1989). A family of mitochondrial proteins involved in bioenergetic CS and biogenesis. *Nature* **339**: 147–149.
- Smith, M.K., Day, D.A., and Whelan, J. (1994). Isolation of a novel soybean gene encoding a mitochondrial ATP synthase subunit. *Arch. Biochem. Biophys.* **313**: 235–240.
- Stroud, D.A., Meisinger, C., Pfanner, N., and Wiedemann, N. (2010). Biochemistry. Assembling the outer membrane. *Science* **328**: 831–832.
- Stuart, R.A. (2008). Supercomplex organization of the oxidative phosphorylation enzymes in yeast mitochondria. *J. Bioenerg. Biomembr.* **40**: 411–417.
- Sunderhaus, S., Klodmann, J., Lenz, C., and Braun, H.P. (2010). Supramolecular structure of the OXPHOS system in highly thermogenic tissue of *Arum maculatum*. *Plant Physiol. Biochem.* **48**: 265–272.

- Thimm, O., Bläsing, O., Gibon, Y., Nagel, A., Meyer, S., Krüger, P., Selbig, J., Müller, L.A., Rhee, S.Y., and Stitt, M.** (2004). MAPMAN: A user-driven tool to display genomics data sets onto diagrams of metabolic pathways and other biological processes. *Plant J.* **37**: 914–939.
- Truscott, K.N., Kovermann, P., Geissler, A., Merlin, A., Meijer, M., Driessen, A.J., Rassow, J., Pfanner, N., and Wagner, R.** (2001). A presequence- and voltage-sensitive channel of the mitochondrial preprotein translocase formed by Tim23. *Nat. Struct. Biol.* **8**: 1074–1082.
- van der Laan, M., Wiedemann, N., Mick, D.U., Guiard, B., Rehling, P., and Pfanner, N.** (2006). A role for Tim21 in membrane-potential-dependent preprotein sorting in mitochondria. *Curr. Biol.* **16**: 2271–2276.
- Wever, W., McCallum, E.J., Chakravorty, D., Cazzonelli, C.I., and Botella, J.R.** (2010). The 5' untranslated region of the VR-ACS1 mRNA acts as a strong translational enhancer in plants. *Transgenic Res.* **19**: 667–674.
- Whelan, J., Hugosson, M., Glaser, E., and Day, D.A.** (1995). Studies on the import and processing of the alternative oxidase precursor by isolated soybean mitochondria. *Plant Mol. Biol.* **27**: 769–778.
- Wittig, I., and Schägger, H.** (2009). Supramolecular organization of ATP synthase and respiratory chain in mitochondrial membranes. *Biochim. Biophys. Acta* **1787**: 672–680.
- Zerbetto, E., Vergani, L., and Dabbeni-Sala, F.** (1997). Quantification of muscle mitochondrial oxidative phosphorylation enzymes via histochemical staining of blue native polyacrylamide gels. *Electrophoresis* **18**: 2059–2064.